A degron-based bioPROTAC for controlling signaling in CAR T cells

by
Matthew Kim

DISSERTATION
Submitted in partial satisfaction of the requirements for degree of
DOCTOR OF PHILOSOPHY

in

Biochemistry and Molecular Biology

in the

GRADUATE DIVISION
of the
UNIVERSITY OF CALIFORNIA, SAN FRANCISCO

Approved:

DocuSigned by:
Tanja Kortemme
74ABEB009F65402...
Tanja Kortemme
Chair

DocuSigned by:
Hana El-Samad
Hana El-Samad

DocuSigned by:
Wendell Lim
3901952758864EF...
Wendell Lim

Committee Members

Acknowledgements

The long journey to completing a PhD is physically, mentally and emotionally taxing. At certain points, I did not think I would be here writing this thesis. The support of friends, family and colleagues was pivotal in reaching the finish line. This section of my thesis is dedicated to everyone that played a role in me becoming the person and scientist I am today.

I would like to thank my family first and foremost. As a kid, my parents were always working. They worked hard so that my brother and I could have dreams. The sacrifices they made for us are unfathomable and without them I would not be where I am today. I am grateful to have them as parents and none of my accomplishments would have been possible without their undying support and love. I am fortunate to have my brother, my cousins, my aunts and uncles here with us in the United States and I appreciate all their support over these almost 3 decades of my life. Without my family being who they are, I could never have been able to achieve my goals and be writing my thesis now.

My grandfather played a huge role in my life. He was always there for me whenever I needed and was the most generous person I have ever known. Sadly, he passed before I started grad school, but I hope that I continue to make him proud.

Next, I would like to thank my Tetrad classmates who are all incredible scientists and even better people. I feel extremely fortunate to have met you all and to have gone through the PhD adventure together. I would especially like to thank Harold, Hayden, Jesslyn, Lorenzo, Megan, Seesha, and Wei for their friendship. Thank you for all for being kind and supportive friends.

I would also like to thank my friends from undergrad as they kept me balanced during my PhD. After over a decade of being friends, it has been a wild adventure and I appreciate every one of you.

All the science I got done during my PhD could not have been possible without my advisor Hana El-Samad. Before coming to grad school, I knew of Hana as a great scientist who did amazing work in synthetic biology. All these years working with her has shown me that she is much more than that. Hana is the type of person that does what they want and fights for their goals. I aspire to be that type of scientist and I am lucky to have been able to meet and work with Hana at UCSF. Hana also has an unbelievable work ethic. It is inconceivable how much Hana can get done in a day. Her passion for her work really drove the lab to be their best. I have learned so much from Hana and my growth as a scientist would not have been the same without her.

I would also like to thank Andrew Ng for being a secondary advisor to my PhD. The only person that works as much as Hana is Andrew. Somehow, he was able to work his industry job, get married, and have kid while still being able to help me out and give me incredibly helpful feedback on my work. Andrew is incredibly generous with his time and was always there when I needed help. Although we did not always agree on where to take the project or how things in our paper should look, he was patient and kind throughout all of it. Working with Andrew has helped me grow tremendously as a scientist.

I cannot express how thankful I am for the people in the El-Samad lab. Hersh, Sarah, Seesha and Zara were the members of the lab as I finished my degree. Thanks, Hersh for being a

meticulous and driven scientist. Your presence in the lab was much appreciated and it was great working together. Thanks, Sarah for being so reliable and so hard working. Your ambition and work ethic are admirable. Thanks, Zara for being Dr. Weinberg. Your dedication and passion for science is an inspiration. Thanks again to Seesha. I have never met someone as multifaceted as Seesha and it was amazing to see her doing science and all the other things she is great at. I would also like to thank Alain and Lindsey who were senior students when I joined the lab. Their wisdom about both science and life were incredibly helpful during my time at UCSF. They are incredibly brilliant and hard-working scientists who fostered a fun lab environment at all times of the day. My time in the lab would not have been the same without all of you and your advice and comments about science and beyond were a joy every day.

Thank you, Tanja and Wendell, for the support you have given me throughout the years. Thank you, Tanja, for being kind and calm during the chaos of my thesis meetings. Thank you, Wendell, for everything you have done for me and giving me the opportunity to grow as a scientist through CDI.

Next, I would like to thank Wendell's lab and the Cell Design Institute for giving me another home at UCSF during the latter years of my PhD. I learned everything about doing T cell work from them and this thesis would not have been possible without your help. I would like to thank Ki, Nick, Devan and Riley for their friendship and their help both in and out of lab. I would like to thank Milos for all his helpful advice regarding science and beyond and being a co-mentor for Rudy during his Master's work. It was a pleasure working with you. I would like to

thank Ricardo and Greg for all their advice on my work. The fellowship that CDI provides is unparalleled and was essential to completing my PhD.

I need to thank all the people that kept the El-Samad lab, the Lim lab and CDI running. I sincerely thank Sim and Pilar for all the work they do. You both always had all the answers and reagents I needed whenever I needed them. You have saved so many of my experiments. Melissa and Detzaira have the hardest job of all. Scheduling Hana for meetings was probably the most difficult part of the PhD and without both of your help it would not have been possible. The same applies to Noleine who helped me get on Wendell's calendar whenever I needed, made sure I got all my logistics taken care and is just overall a great person. Manny deserves a huge thank you as well. Thanks, Manny, for letting me do all the crazy stuff in lab and always being there with support in every capacity.

Thank you to the Tetrad program for being my home during my PhD. I would like to thank Toni, Billy, Veena and Danny for all their help. I also want to take the time to apologize for being delinquent on almost everything during my PhD. I appreciate all your understanding and patience.

Scientific growth and scientific community go hand in hand. I would not have been able to develop as a scientist without the mentorship and community of all the labs I have worked in. Thank you to all the PIs that gave me the opportunity to work in their lab. I especially would like to thank Dr. Dave Savage for taking a chance on me as a second-year undergrad with no lab experience. I also would like to thank Dr. Michael Elowitz, Dr. Xiaojing Gao and Dr. Lucy Chong for giving me the opportunity to work on a great project and for giving me a community

to become a confident scientist. The skills and tools I learned during my time in the lab were key in successfully finishing my degree. Thank you to Dr. Sanjay Sinha for letting me work in your lab. Your passion for science is infectious and it was great learning how you think about science. I would not have been able to be here today without these opportunities.

Finally, I want to thank Mimi. Mimi has supported me throughout the entirety of my career in science. Mimi and I went together to meet my first PI to interview for an undergrad position in his lab. I spent a very long time speaking with everyone in the lab. As I was walking out, Mimi was sitting outside on a bench. She was there the whole time waiting for me. Since then, she has been there for me. Words cannot describe the impact Mimi has had on my life. She is selfless, dedicated, caring, intelligent and so much more. She inspires me every day to work hard and to strive for happiness. Thank you, Mimi, for being with me throughout this journey and I look forward to our future together.

A degron-based bioPROTAC for controlling signaling in CAR T cells

Matthew Kim

Abstract

Genetically engineered therapeutic cells are a new paradigm in treating historically intractable diseases. Chimeric antigen receptor ('CAR') T cells have made a tremendous impact in the clinic against blood cancers, but potent signaling through the CAR can result in toxicity and CAR T cell exhaustion. Further engineering efforts to modulate CAR signaling are needed to continue to deploy engineered cell therapies against increasingly complex maladies. The use of protein degradation to ablate CAR signaling is a promising method for improving CAR T cell safety and efficacy. In preclinical models, small molecule-controlled protein degradation to tightly control CAR expression levels was shown to circumvent issues of CAR T cell toxicity and exhaustion. An equally important complement to small molecule modes of control are genetic circuits that allow therapeutic cells to reactively modulate CAR signaling in response to their environment. Using genetic circuits in combination with protein degradation could result in the birth of a new class of engineered cell therapies capable of cell autonomous regulation of therapeutic function. However, programmable targeted protein degradation tools for this purpose do not exist for immune cell engineering. To address this gap in the existing CAR T cell engineering toolbox, we designed a novel bioPROTAC that uses two protein domains to bridge a target protein of interest with machinery from the ubiquitin proteasome system to promote proteasomal recruitment and degradation. We built the bioPROTAC such that it is capable of degrading both cytosolic and membrane proteins while also being as small as 181 base pairs for

efficient delivery by lentivirus. We show that the bioPROTAC is capable of degrading cytosolic proteins such as green fluorescent protein ('GFP') in multiple mammalian cell lines, as well as degrading and functionally modulating membrane proteins such as second-generation CARs in T cells. To demonstrate our bioPROTAC's ability to be composed into genetic circuits that modulate cell signaling pathways, we engineer an antigen-inducible circuit capable of shutting down CAR signaling through degradation of the tyrosine kinase ZAP70. Through this circuit, we show that this new bioPROTAC can interface with and modulate endogenous signaling networks under user-defined cell autonomous control. Genetic circuits that actuate protein degradation can be a powerful method for engineering self-regulating CAR T cells thereby improving therapeutic safety and efficacy.

Table of Contents

List of Figures

Chapter 1: Introduction

Synthetic biology reimagines cells as living computers with complex circuitry composed of vast networks of interacting macromolecules. At the turn of millennium, synthetic biologists programmed bacterial cells with *de novo* circuitry and taught cells to regulate a specific protein in response to a user-defined stimulus[1,2]. Stemming from these discoveries, the field of synthetic biology continues to expand its toolbox of molecular parts, explore the landscape of circuit topologies and apply these ideas to a larger number of cell types and organisms. Of particular interest is mammalian cell engineering because of the potential to both elucidate the underpinnings of life and improve human health.

Engineered cells are a powerful therapeutic modality that can sense environmental cues, process these cues through genetic circuits, and respond appropriately. This decision-making process offers a new facet to therapeutics that traditional therapies lack. The potential of engineered cell therapies is highlighted by the clinical success of chimeric antigen receptor ('CAR') T cells. CARs are composed of a custom extracellular domain, typically a single chain variable fragment ('scFv'), and signaling domains taken from the T cell receptor and associated co-stimulatory receptors. These synthetic receptors can redirect T cell signaling towards cancer cells, demonstrating complete response in up to 86% of patients with blood cancers that were resistant to other therapeutics such as chemotherapy[3,4]. However, potent and sustained CAR signaling can be a double-edged sword. High levels of CAR T cell activity are associated with cytokine release syndrome ('CRS') resulting in severe inflammation, life-threatening shock and organ failure. Furthermore, chronic activation of the CAR can induce a hypofunctional state known as T cell exhaustion, limiting the therapeutic efficacy of CAR T cell therapies[5,6]. The use

of genetic circuits and small molecule-based approaches to tightly regulate CAR function has shown promising results in improving CAR T cell efficacy and safety in *in vitro* and mouse models.

Genetic circuits enable cell-by-cell decision making to modulate CAR T cell signaling in response to local environmental cues. This signal processing can enhance CAR T cell specificity, efficacy, and safety. One of the earliest and most compelling implementation of genetic circuits in cell therapies are logic gates constructed using antigen-sensing receptors such as synthetic Notch ('synNotch') and Synthetic Intramembrane Proteolysis Receptors ('SNIPR')[7–12]. synNotch and SNIPR convert antigen binding to transcriptional activation of a custom, user-defined payload. By gating CAR expression upon synNotch/SNIPR activation, these circuits control when and where CARs can be active. This control improves CAR T cell specificity and safety in mouse models and has even been shown to improve efficacy through silencing of tonic signaling. Additionally, genetic circuits have been constructed with cell-state promoters or synNotch to drive cytokine production in response to specific cellular contexts to improve CAR T cell tumor clearance[13,14]. These circuits rely on specific cellular interactions to actuate a response thereby restricting control to individual cells. The spatial and temporal confinement of circuit effects prevents wanton lysis of healthy tissue or detrimental CAR signaling while still allowing a population of engineered cells to perform their therapeutic function. Genetic circuits endow engineered cell therapies with new functions and behaviors vastly expanding their therapeutic potential.

The use of the small molecules to shut off TCR pathway signaling can also regulate CAR T cell signaling. Dasatinib is a small molecule inhibitor that downregulates the activity of the Src kinases in the proximal signaling network of the TCR[15]. While this method of modulation works to prevent unwanted CAR signaling, dasatinib is not specific to T cells or specific to kinases in the pathway so the impact of global downregulation of these essential signaling molecules could be detrimental to patient health or therapeutic efficacy. Targeted protein degradation ('TPD') is a promising alternative method of modulating cell signaling and, in some cases, can be more effective than inhibition through the complete removal of proteins in the signaling pathway[16]. Indeed, small molecule controlled degrons have been used to regulate CAR expression and can be used to modulate CAR signaling in pre-clinical models. Degrons under the control of the small molecule lenalidomide has been used to specifically degrade CARs with high temporal precision. This precise temporal ablation of CAR signaling prevents detrimental CAR signaling with implications in preventing healthy tissue lysis and CRS[17,18]. Similarly, another work demonstrated that degradation of CARs can not only prevent exhaustion but can also rescue CAR T cells that have already succumbed to exhaustion[16,19]. This is a powerful application of degradation as a mode CAR T cell signaling modulation because it is the first demonstration that CAR T cell exhaustion is reversible and demonstrates that dynamic regulation of CAR expression is essential for promoting CAR T cell health and therapeutic efficacy.

A yet unexplored method for modulating CAR T cells is the marriage of genetic circuits and targeted protein degradation. Using the sophisticated signal processing afforded by genetic circuits and coupling them with the potent modulation of protein degradation, CAR T cell

therapies could be vastly improved. However, the methods for controlling CARs in previous studies are not amenable to regulation by genetic circuits. Therefore, a new mode of degrading CARs, or CAR associated proteins, is needed to accomplish this union.

An alternative method of inducing degradation of a protein of interest ('POI') is the use of protein-based heterobifunctional molecules known as bioPROTACs. bioPROTACs are composed of one protein domain that binds a POI and another protein domain that promotes ubiquitylation of the POI[20–24]. 'Ubiquibodies' were one of the first demonstrations that a protein-based heterobifunctional model of bioPROTACs can be a viable protein degrader in mammalian systems. Recently, a systematic exploration of this bioPROTAC design demonstrated that domain swapping of either the target recognition or UPS recruitment domains can alter function. Interestingly, bioPROTACs were shown to be modular molecules that can use a variety of target binding domains, including truncations of endogenous proteins, to induce degradation thereby greatly expanding the space of potential POIs[20–24]. Furthermore, another tool, coined 'nanodeg', showed that a short degron sequence can replace the UPS recruitment domain and still achieve strong degradation of a POI. bioPROTACs are potentially powerful tools for cell engineering because they require minimal or no protein engineering of the POI, can be easily designed to target different POIs via domain swapping and are genetically encodable, enabling their composition into genetic circuits. Taking advantage of the genetically encodable nature of bioPROTACs, we envisioned the development of genetic circuits that degrade either synthetic or endogenous signaling proteins to modulate cellular responses based on environmental cues.

An ideal bioPROTAC for constructing genetic circuits would have potent degradation activity against a variety of different cellular targets and be compact in size to enable efficient delivery as genetic payloads. Taking these considerations into account, we developed a novel compact bioPROTAC and demonstrated its functionality in primary human CAR T cells. We tested a variety of different protein binding domains including the SynZip protein interaction toolkit. This bioPROTAC is a heterobifunctional molecule that can be as small as 181 base pairs and can degrade both cytosolic and membrane proteins. When targeted to a CAR, our bioPROTAC degraded over 99% of CAR protein on the T cell surface and abrogated CAR related T cell signaling against target cells *in vitro*. We coupled our technology with CRISPR/Cas9 knock-in methods and the transcriptional activating receptor SNIPR to tag and degrade the endogenous ZAP70 protein in response to a stimulus. Using this method, we demonstrated our bioPROTAC can be composed into a circuit that uses specific intercellular interactions to elicit degradation and modulate CAR signaling. This use of programmable protein degradation circuits based on our bioPROTAC provides a powerful method to dictate engineered cell behavior and function. The incorporation of synthetic cell-autonomous protein degradation to both synthetic and endogenous protein networks could be a new paradigm in immune cell engineering.

Chapter 2: Novel bioPROTAC potently degrades cytosolic proteins

Targeted protein degradation can be achieved by recruiting the ubiquitin proteasome system ('UPS') to a protein of interest via heterobifunctional molecules that combine a target recognition domain with a UPS recruiting domain (Fig 1A). In this work, we optimized a bioPROTAC for cell engineering by minimizing the UPS recruiting domain in the form of a degron, enhanced activity through rational protein engineering, and demonstrated broad utility in human T cells.

Most existing bioPROTACs utilize full length or truncated E3 ubiquitin ligases to recruit the UPS. This approach is not favorable for cell engineering because E3 ubiquitin ligases and their domains can be quite large, posing a potential challenge for delivery of the genetic material into the cell[25]. In this work, we explored the use of degrons to recruit the UPS because of their smaller genetic payload size. This is essential for our goal of constructing complex genetic circuits as efficient genetic payload delivery in T cells is negatively correlated with payload size[26]. We first screened previously published degron sequences known to promote ubiquitylation and degradation by fusing these degrons to the C-terminus of GFP. We then measured GFP fluorescence in Jurkat cells by flow cytometry to assess degron efficacy[27–30]. From these data, we found that the Bonger LID degron induced over 116-fold decrease in GFP fluorescence relative to a reporter only control, the highest in our screen (Fig 1B). The compact size of the Bonger LID degron, comprising only four residues ('RRRG'), also makes it ideal for applications in constructing a cell engineering focused bioPROTAC. Future experiments in this work will simply refer to the Bonger LID degron as "degron".

Next, we wanted to test if the degron could induce *trans* degradation of GFP as a model target protein. We hypothesized that bringing our degron within close proximity of GFP would promote ubiquitylation and degradation of GFP through degron-based recruitment of endogenous E3 ubiquitin ligases. In addition to testing a vhhGFP4 anti-GFP nanobody as a binding domain, we explored the use of synthetic leucine zippers ('SynZips') as alternative binding domains. SynZips are a powerful tool for cell engineering due to their compact size, well-characterized affinity and orthogonality[31,32]. We fused either a SynZip or the vhhGFP4 nanobody to the degron via a short, flexible GS repeat linker to generate bioPROTACs. As a "no degron" negative control, we substituted the degron in this design for the peptide sequence 'TRGN' that demonstrates no degron activity[27]. To test our bioPROTACs, we lentivirally co-transduced Jurkat T cells with one plasmid encoding a GFP target protein and another encoding either the SynZip or nanobody bioPROTAC. Recruitment of the SynZip bioPROTAC required tagging the GFP with a C-terminal fusion of the cognate SynZip. We tested SynZip17 and its cognate SynZip18, SynZip1 and its cognate SynZip2, and the vhhGFP4 nanobody for bioPROTAC recruitment. We then measured GFP fluorescence by flow cytometry. To assess degradation efficacy of each bioPROTAC variant, we calculated "Relative GFP fluorescence" which is GFP fluorescence of each condition normalized to the fluorescence of GFP alone. While some designs exhibited strong degradation, others, the nanobody in particular, showed as little as 1.45-fold reduction in GFP fluorescence (Fig 2). We hypothesized that cis-ubiquitylation could be limiting the activity of the bioPROTAC by inducing degradation of the bioPROTAC in addition to the POI.

Previous work has shown that mutating lysine residues of a TPD tool can improve its activity by minimizing cis-ubiquitylation of the bioPROTAC and enhancing trans-ubiquitylation of the POI[33]. We applied this logic to our initial designs by replacing lysine residues on the binding domain with arginine ('K ->R mutation'). By performing the lysine substitution on the SynZip18 binder, we observed a 12-fold increase in activity over the wild-type binder and a 60-fold decrease in GFP fluorescence relative to the no degron control (Fig 1C). We observed a 100-fold increase in activity over the wild-type binder and a 204-fold decrease in GFP fluorescence relative to the no degron control with the mutated nanobody bioPROTAC (Figure 1D). This optimized bioPROTAC incorporating either SynZip18 or vhhGFP4 nanobody with K->R mutations fused to the RRRG degron is the foundation for all the experiments used in this work.

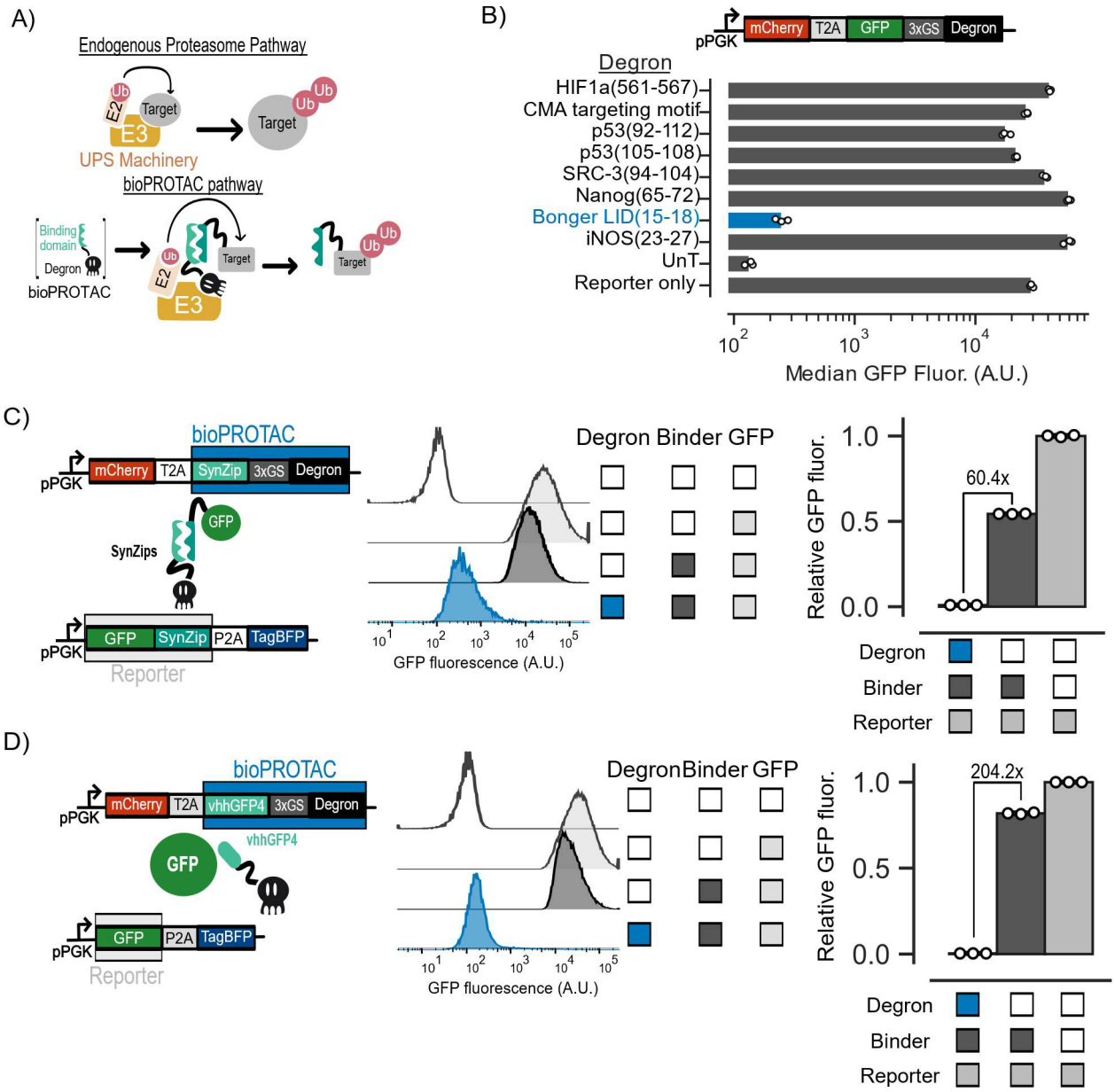

Figure 1. Novel bioPROTAC potently degrades cytosolic proteins (A) Mammalian cells coordinate a majority of protein flux through the ubiquitin proteasome system. The UPS serves as a foundation for bioPROTACs with target binding, UPS component recruitment and ubiquitylation sites as potential knobs for optimization and tuning of target degradation. (B) In a small screen of degrons in Jurkat cells, the 4 amino acid sequence 'RRRG' acted as the most potent degron and was adopted as the UPS recruitment motif for our bioPROTAC in all subsequent experiments. Reporter fluorescence was assayed by flow cytometry. Dots represent technical replicates and error bars show SEM. (Figure caption continued on the next page)

(Figure caption continued from the previous page) (C and D) Design strategies based on synthetic leucine zippers ('SynZips') and the vhhGFP4 nanobody are both capable of recruiting bioPROTACs for potent degradation of GFP. Left: Jurkat T cells were lentivirally co-transduced with plasmids encoding a bioPROTAC and a mCherry tranduction marker and a GFP reporter protein with a BFP transduction marker. Middle: Flow cytometry histograms of the diagramed plasmids in the left panel alongside controls. We substitute the degron sequence for the sequence 'TRGN' that exhibits no degradation capability. This "no degron" control serves as a negative control for recruitment of the UPS and degradation which is represented by the dark gray histograms. Histograms are representative of three independent experiments. Right: Quantification of flow cytometry histograms. GFP fluorescence of each condition was normalized to the reporter only condition (light gray bar). Relative GFP fluorescence was calculated by normalizing measured GFP fluorescence by the fluorescence of the reporter only control. Each dot represents a technical replicate and error bars show SEM.

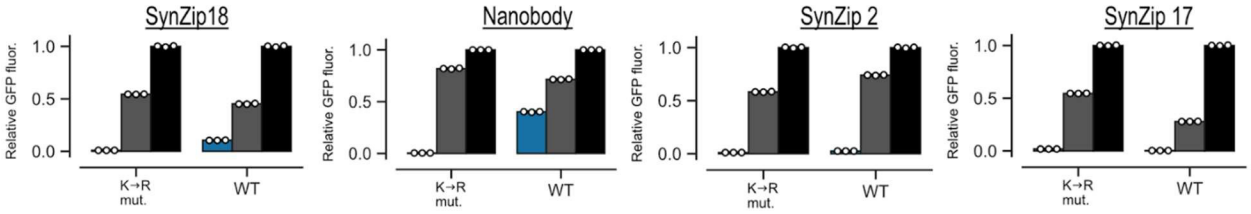

Figure 2. bioPROTAC degradation improves upon mutation of lysine residues to arginine. Mutation of the lysine residues to arginine in the binding domain of bioPROTACs improves degradation of GFP. We compare the ability of mutated and wildtype binders to recruit to and degrade a GFP target. The SynZip18 and nanobody variants of bioPROTACs benefit the most from these mutations. Dots are representative of technical replicates and error bars show SEM. Relative GFP fluorescence was calculated by normalizing measured GFP fluorescence by the fluorescence of the reporter only control.

Chapter 3: Novel bioPROTAC is a versatile tool that functions through the UPS and cullin ring ligases

To determine whether our bioPROTAC can function in different cell types, we tested them in mouse embryonic stem cells ('mESCs'), primary human CD4+ T cells, 3T3 mouse fibroblasts, HEK293T cells and K562 leukemia cells by co-transducing a GFP reporter and either a nanobody or SynZip based bioPROTAC. We found that the bioPROTAC utilizing the SynZip binding domain reduced GFP fluorescence by over 33-fold relative to reporter only controls in all tested cell types, demonstrating the versatility of our bioPROTAC for cell engineering (Fig 3A). The nanobody variant of the bioPROTAC produced similar fold changes in these cell lines (Fig 4E).

To understand the mechanism of GFP degradation via the bioPROTAC, we used a small molecule panel to interrogate the proteasomal and lysosomal pathways. Jurkat T cells were engineered with the plasmids described in Figure 1C and then treated with either the proteasomal inhibitor MG-132, the vacuolar ATPase inhibitor Bafilomycin A1, the pan cullin ring ligase inhibitor MLN4924 or a DMSO control for 5 hours in a tissue culture incubator. After treatment, cells were washed and analyzed for GFP fluorescence by flow cytometry. We observed minor rescue of GFP fluorescence in cells treated with MG-132 and much higher levels of rescue in cells treated with MLN4924 relative to a DMSO vehicle control. As expected, GFP fluorescence was not affected in cells treated with Bafilomycin A1 as we did not predict any contribution by the lysosome for bioPROTAC induced degradation of GFP. These data suggest that the bioPROTAC-dependent loss of GFP fluorescence is due to protein degradation through the UPS mediated by cullin ring ligases (Fig 3B). To further investigate the mechanism of bioPROTAC-

dependent GFP loss, we co-expressed a series of dominant negative cullin constructs to inhibit endogenous cullin function[34]. The dominant negative cullins are unable to promote ubiquitin conjugation to a POI thereby blunting degradation through specific cullin pathways. In these data, we observed a rescue of GFP fluorescence when the bioPROTAC is co-expressed with a dominant negative cullin from the cullin 4A and 4B families, suggesting the RRRG degron is recognized by a cullin ring ligase belonging to this family of cullins in T cells (Fig 4A).

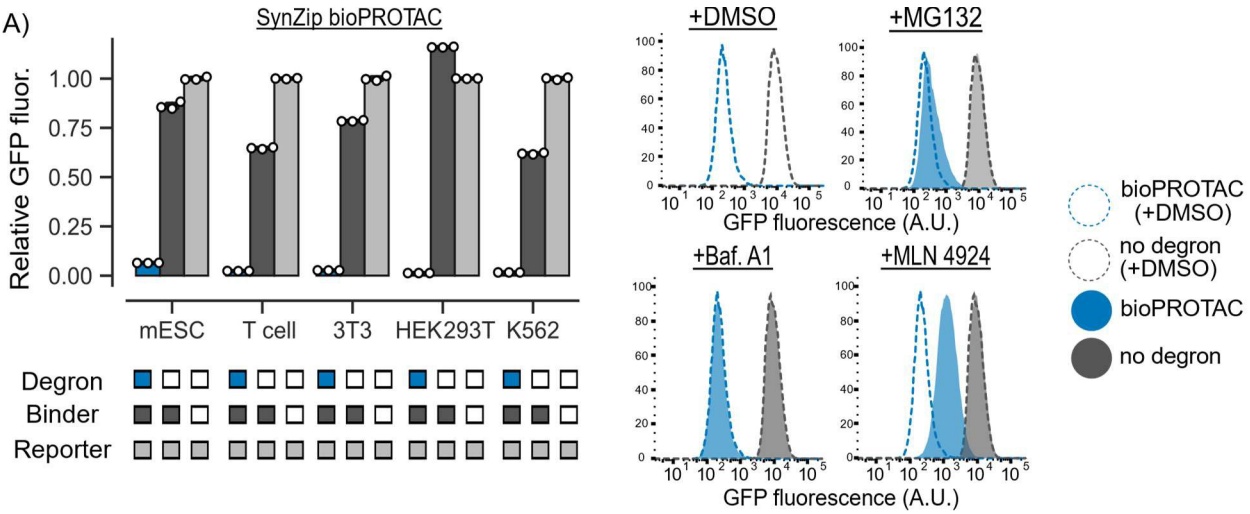

Figure 3. bioPROTAC relies on proteasomal degradation aided by cullin ring ligases (A) bioPROTACs are capable of potent degradation across all tested mammalian cell lines. bioPROTAC efficacy was measured by flow cytometry and normalized to a GFP reporter alone for each cell type. Each dot represents a technical replicate and error bars show SEM. (B) bioPROTAC degradation of cytosolic proteins relies on the proteasome via cullin ring ligases. bioPROTAC and GFP reporter expressing Jurkat T cells or control lines were treated with either 5 uM of the proteasomal inhibitor MG-132, 1 uM of the vacuolar ATPase inhibitor Bafilomycin A1, 100 nM of the pan cullin ring ligase inhibitor MLN4924 or a DMSO control for 5 hours at 37 C. Cells were then washed and GFP fluorescence was measured by flow cytometry. Histograms are representative of three biological replicates.

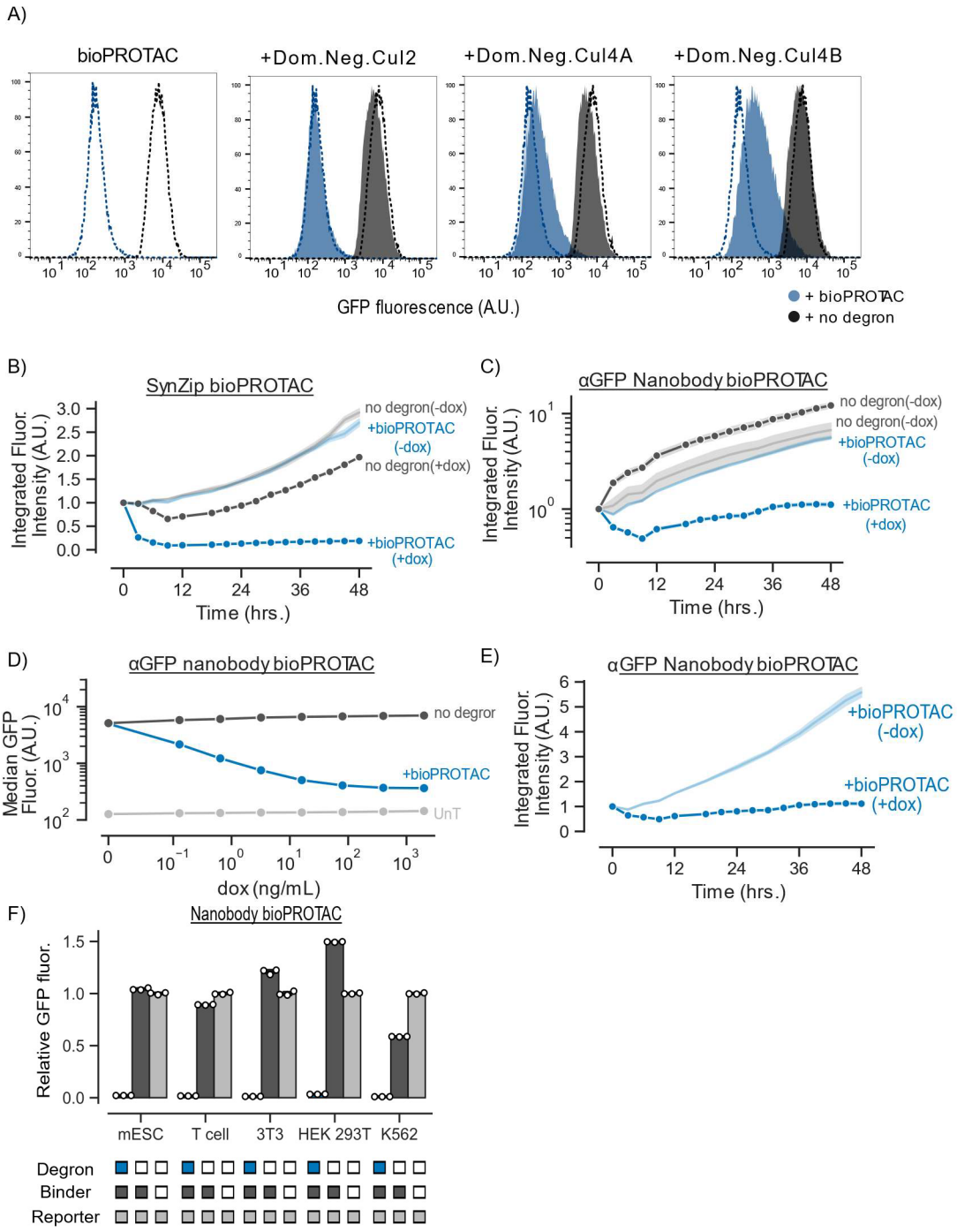

Figure 4. Characterization of bioPROTAC mechanism and function. (A) Dominant negative cullin ring ligases from the CUL 4A and 4B families inhibited bioPROTAC degradation. Dominant negative cullins that do not promote ubiquitylation are introduced with bioPROTACs and GFP. (Figure caption continued on the next page)

(Figure caption continued from the previous page) We find that only the dominant negative variants of CUL4A and CUL4B rescue GFP fluorescence in the presence of bioPROTACs while the dominant negative CUL2 does not. (B) Time traces of SynZip bioPROTAC degradation with additional controls. We observe degradation by bioPROTACs as early as 4 hours post drug treatment. In addition, only the +bioPROTAC(+dox) condition showed a loss in GFP fluorescence during the time course of the experiment. (C) Time traces of nanobody bioPROTAC degradation. We observed that the +bioPROTAC(+dox) condition has dramatically lower GFP fluorescence relative to controls. However, we noted that there is minimal change relative to the initial time point. (D) Nanobody bioPROTAC also showed dose-dependent degradation. bioPROTACs titration resulted in dose-dependent degradation of cytosolic proteins. Jurkat T cells were lentivirally transduced with a GFP reporter protein and a plasmid encoding a doxycycline inducible nanobody bioPROTAC and the Tet3G protein. After isolation by FACS, cells were treated with a 2-fold titration series of dox starting at 2000 ng/mL or a media only control for 48 hours. bioPROTAC efficacy was assessed by flow cytometry. Each dot is the mean of three biological replicates. Error shows SEM. (E) Nanobody bioPROTAC showed potent degradation across all tested mammalian cell lines. bioPROTAC efficacy was measured by flow cytometry and normalized to a GFP reporter alone for each cell type. Dots represents technical replicates and error bars show SEM.

Chapter 4: Kinetics of bioPROTAC mediated degradation

Next, we explored the relationship between bioPROTAC expression level and bioPROTAC-mediated degradation. Jurkat T cells were engineered to express a constitutive GFP reporter protein and doxycycline-inducible expression of the bioPROTAC. We titrated bioPROTAC expression with a serial dilution of doxycycline and measured GFP fluorescence via flow cytometry after 48 hours of treatment (Fig 5A). To better understand the relationship between bioPROTAC concentration and activity, we plotted GFP fluorescence versus BFP fluorescence (BFP being a proxy for bioPROTAC expression) for cells treated with 500 ng/mL doxycycline. At intermediate BFP expression levels, the GFP signal was bimodal, with a small number of cells that retained high GFP expression and a majority of cells that had low GFP expression. At high BFP expression levels, GFP fluorescence was completely ablated, indicating bioPROTAC activity is thresholded on expression level (Fig. 5A). We also observed dose-dependent degradation with the nanobody bioPROTAC under similar experimental conditions (Fig 4D).

In order to explore the kinetics of bioPROTAC-mediated degradation, we next treated cells with a saturating dose of 2000 ng/mL doxycycline and measured GFP intensity over 48 hours using fluorescence microscopy and live cell imaging. We observed loss of GFP fluorescence within 3 hours, and complete degradation of GFP within 12 hours while the untreated control demonstrated increasing GFP fluorescence over the course of the experiment associated with cell proliferation and growth (Fig. 5B and 4B). The kinetics of bioPROTAC degradation are comparable to that of previously published tools such as nanodeg, but slower than other published bioPROTACs that can pre-complex with their POI, such as the mAID-

nanobody, prior to activation[13,33]. The doxycycline induced nanobody bioPROTAC showed a 6-fold reduction in GFP fluorescence over time relative to an untreated control. However, we did not observe meaningful changes relative to the initial time point. We hypothesize that this phenomenon may be due to the ability of the nanobody to enhance GFP fluorescence (Fig 4C and E). We observed this characteristic in our experiments as the no degron control showed the highest level of fluorescence.

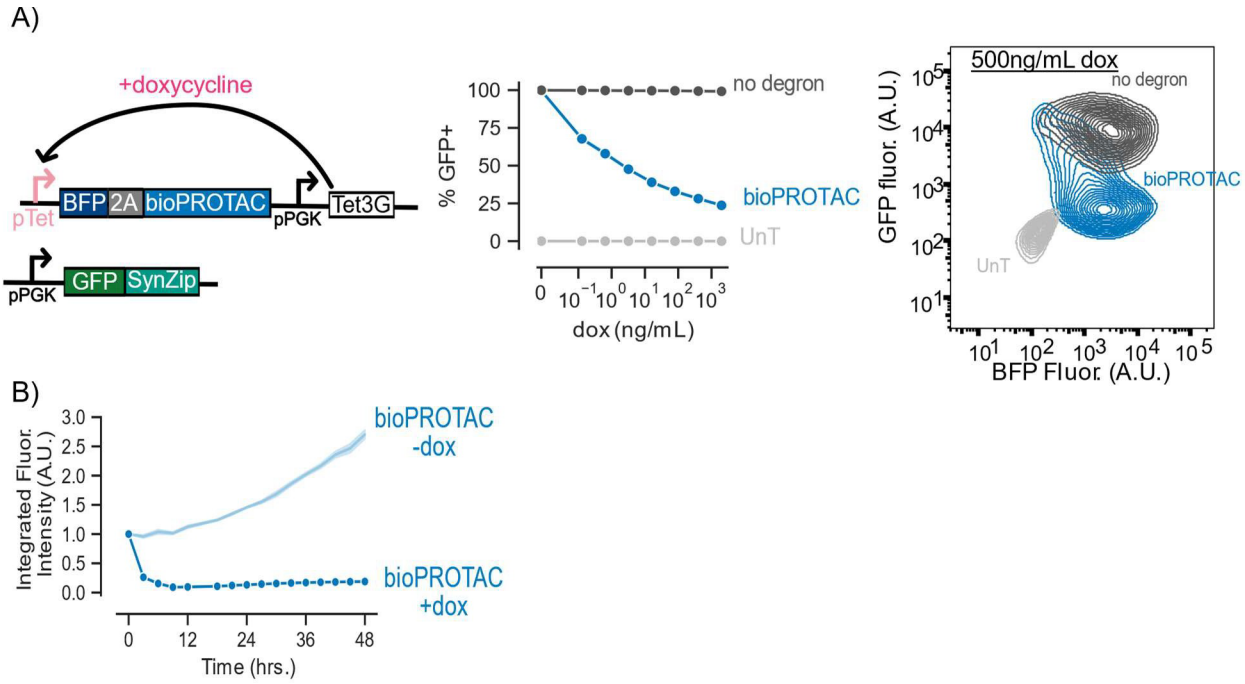

Figure 5. bioPROTAC degradation is dose-dependent and rapid. (A) bioPROTAC titration results in dose-dependent degradation of cytosolic proteins. Left: Jurkat T cells were lentivirally transduced with a GFP reporter protein and a plasmid encoding a doxycycline inducible bioPROTAC and the Tet3G protein. Middle: After isolation by FACS, cells were treated with a 2-fold titration series of dox starting at 2000 ng/mL or a media only control for 48 hours. bioPROTAC efficacy was assessed by flow cytometry. Each dot is the mean of three biological replicates. Error shows SEM. Right: Representative countour plot of bioPROTAC expression level (BFP) and GFP expression level at 500 ng/mL of doxycycline. (Figure caption continued on the next page)

(Figure caption continued from the previous page) (B) bioPROTACs exhibited substantial loss in GFP after 4 hours of doxycycline treatment. The doxycycline inducible Jurkat T cells line described above was treated with either 2000 ng/mL doxycycline or a media only control and incubated for 1 hour at 37 C. Then, cells were imaged on an Incucyte instrument every 3 hours for 48 hours. Each trace is normalized to integrated fluorescent intensity values at the initial measurement time point. Each dot is the mean of three biological replicates. Error shows SEM.

Chapter 5: Plasma membrane localization of bioPROTAC enhances CAR degradation

We next set out to test whether bioPROTACs could induce degradation of CARs, which are transmembrane proteins. Jurkat T cells were lentivirally transduced with a single plasmid encoding a transduction marker, bioPROTAC, and a CAR separated by 2A elements to assess bioPROTAC degradation of the CAR (Fig 6A). To allow for bioPROTAC recruitment and subsequent degradation, we fused a SynZip to the C-terminus of the CAR. For simplicity, we will still refer to this modified fusion molecule as a CAR. We tested bioPROTAC induced degradation of two second-generation CAR variants, an anti-CD19 4-1BBz CAR and an anti-HER2 4-1BBz CAR. We used flow cytometry to measure surface expression of the CAR molecules after staining for an epitope tag fused to the CAR. To assess degradation efficacy, we quantified the percentage of CAR remaining at the cell surface as a function of the background subtracted CAR fluorescence normalized to the CAR only control. We found that the bioPROTAC exhibited minimal effect on anti-HER2 CAR expression, but reduced anti-CD19 CAR fluorescence by 80%. Despite the reduction in CAR fluorescence, substantial anti-CD19 CAR expression was still detectable at the cell surface. Previous work has demonstrated that low levels of CAR expression in CAR T cells can still result in complete clearance of tumor cells *in vitro*[35]. We therefore sought to improve bioPROTAC activity to maximize CAR degradation and minimize any potential signaling.

We hypothesized that increasing the local concentration of the bioPROTAC at the plasma membrane could mediate more efficient degradation of target membrane proteins. We used a previously described chimeric DAP10-CD8a membrane tethering domain or a lyn membrane targeting tag and fused it to the bioPROTAC via a rigid 15 amino acid linker to create a new

molecule. To differentiate this molecule from our previously described design, we will refer to it as the membrane tethered bioPROTAC or 'membioPROTAC'[36,37]. We, accordingly, renamed the original, non-tethered design the "cytosolic bioPROTAC". We compared the activity of the cytosolic bioPROTAC, the membioPROTAC and a no degron control for the membioPROTAC where the degron is swapped degron for the peptide sequence 'TRGN'. We again lentivirally transduced Jurkat T cells with a single plasmid encoding a GFP transduction marker, bioPROTAC, and a CAR separated by a 2A element to assess for bioPROTAC degradation of the anti-CD19 and anti-HER2 CAR. When paired against an anti-HER2 CAR, the membioPROTAC degraded 86% of detectable CAR representing a substantial improvement over the cytosolic bioPROTAC (Fig 6B and 6D). Similarly, the membioPROTAC augmented degradation of the anti-CD19 CAR by more than 20% relative to the cytosolic bioPROTAC resulting in an over 99% degradation of the anti-CD19 CAR relative to the CAR alone control (Fig 6C and 6D). Interestingly, we observed that the bioPROTAC, despite membrane localization, showed lower levels of degradation against both the antiCD19 and antiHER2 CD28z CARs (Fig 7A). We observed similar degradation using the lyn tag variant of the membioPROTAC suggesting that membrane targeting through various mechanisms maintains membioPROTAC function and potency (Fig 7B). We decided to continue future experiments with the DAP10 localized bioPROTAC because the DAP10-based domain allows for detection of bioPROTAC expression through antibody staining of a peptide tag fused to the extracellular domain.

In order to investigate the mechanism of membioPROTAC mediated degradation, we lentivirally transduced Jurkat cells with the plasmids described above, treated these cells with the previously described proteasomal and lysosomal inhibitors and measured CAR expression by flow cytometry. CAR expression was rescued by MLN4924 and unaffected by Bafilomycin A1. Unlike with the cytosolic bioPROTAC, MG132 had minimal effect on membioPROTAC mediated CAR degradation (Fig 6E). This result suggests that internalization of the CAR from the plasma membrane may be mediated through cullin ring ligases, but not the proteasome.

From these data, we concluded that the membioPROTAC degrades CARs in a model of human T cells, but the level of degradation we observed had no bearing on the functional consequences of this degradation. We thus decided to explore the impact of membioPROTAC mediated CAR degradation on CAR T cell activity in primary human T cells.

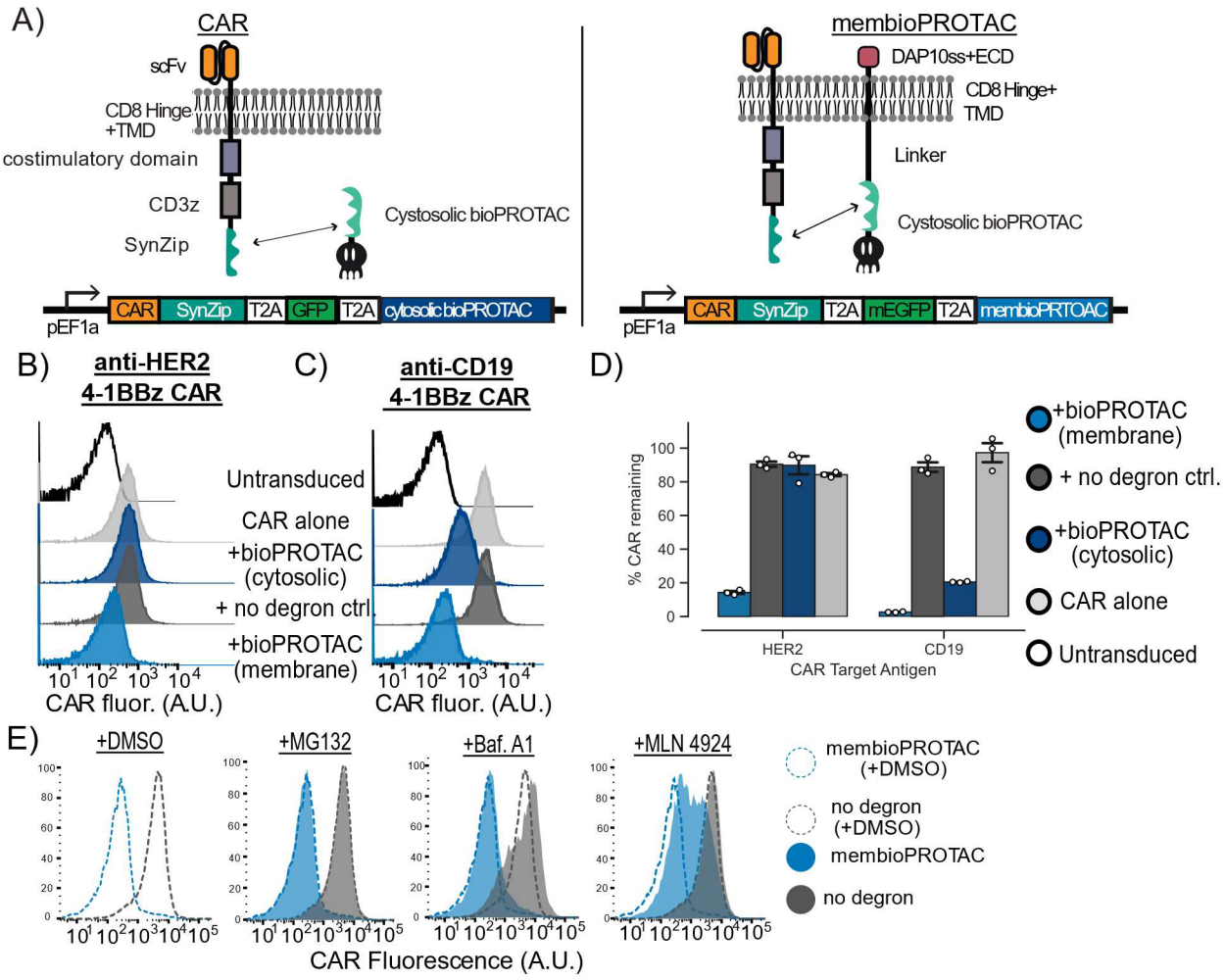

Figure 6. Localization of bioPROTAC to the plasma membrane allows for knockdown of second-generation chimeric antigen receptors in Jurkat T cells (A) Membrane localization of the bioPROTAC improves membrane protein degradation. We hypothesized that localization of the bioPROTAC to the membrane could improve bioPROTAC degradation of membrane proteins, namely a second-generation CAR. Here, we diagram various constructs and controls used to validate this hypothesis. (B) Membrane tethered bioPROTAC ('membioPROTAC') is capable of degradation of a second-generation anti-HER2 4-1BBz CAR. Flow cytometry histograms using the plasmids demonstrating knockdown of anti-HER2 CAR in Jurkat T cells. Histograms are representative of three technical replicates. (C) membioPROTAC is capable of potent degradation of anti-CD19 4-1BBz CAR with some effect from the cytsolic bioPROTAC. Flow cytometry histograms representing Jurkat T cells expressing the plasmids diagrammed in Figure 6A. Histograms are representative of three technical replicates. (D) Quantification of flow cytometry data. % CAR remaining is calculated as background subtracted CAR fluorescence normalized to the CAR alone control. Each dot here represents technical replicates. (Figure caption continued on the next page)

(Figure caption continued from the previous page) (E) Cullin ring ligases are implicated in CAR degradation by membioPROTAC, but not the proteasome. The anti-CD19 CAR Jurkat T cells lines described above were treated with either 5 µM of MG-132, 1 µM MLN4924, 100 nM Bafilomycin A1, or a DMSO vehicle control and incubated at 37 C for 5 hours. Cells were then washed and CAR fluorescence was measured by antibody staining and flow cytometry. Histograms are representative of three biological replicates.

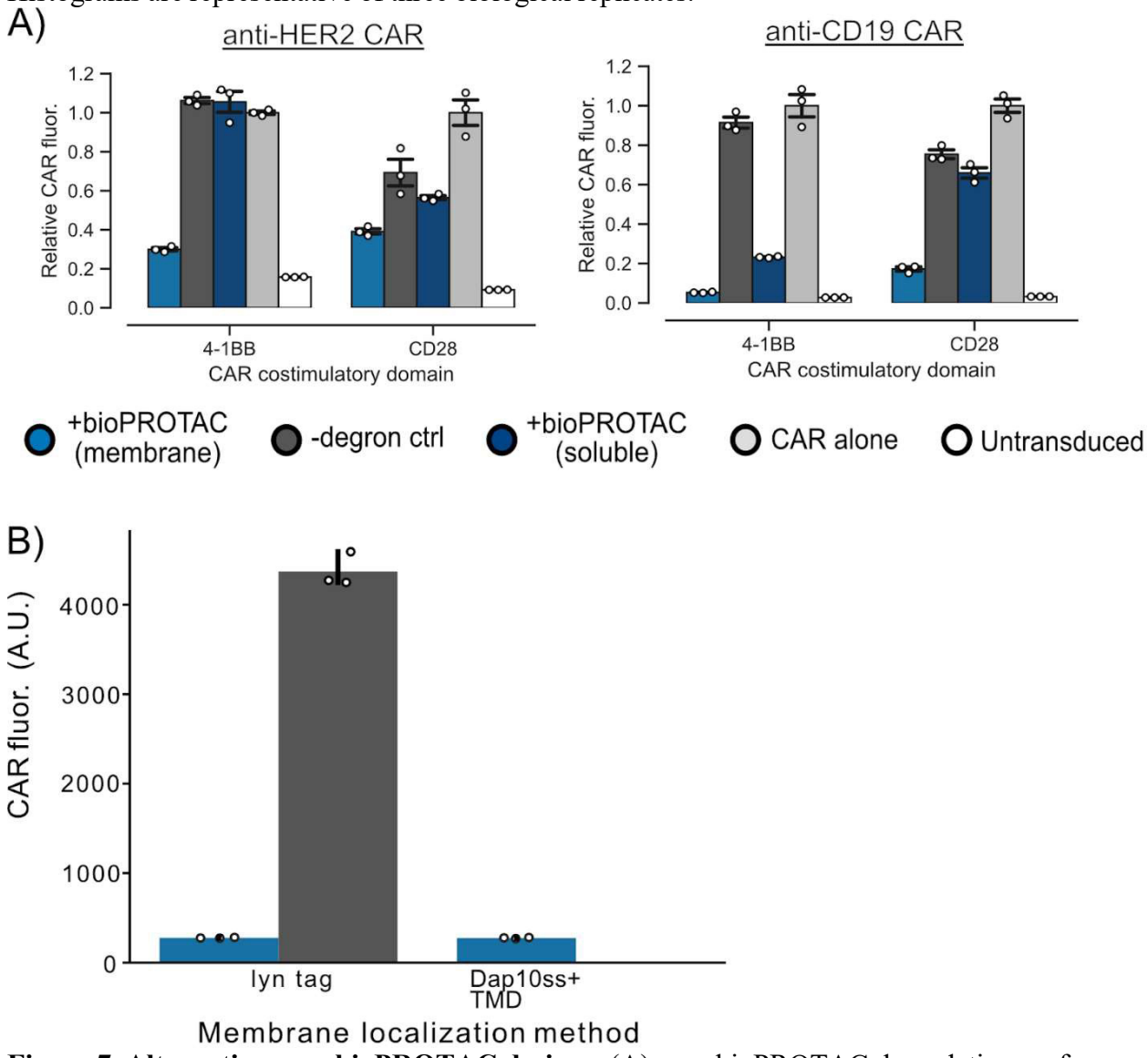

Figure 7. Alternative membioPROTAC designs. (A) membioPROTAC degradation performs better against second-generation CARs with 4-1BB than those with CD28 costimulatory domains. Jurkat T cells lentivirally were transduced with plasmids encoding a second-generation CAR and a membioPROTAC as described in Figure 3A. (Figure caption continued on the next page)

(Figure caption continued from the previous page) CAR expression was measured by staining for an extracellular tag fused to the extracellular domain of the CAR followed by flow cytometry. (B) membioPROTAC can be recruited to the membrane with different domains without loss of function. Jurkat T cells were engineered to express an antiCD19 4-1BB CAR. Then, either a lyn tagged membioPROTAC, a lyn tagged no degron control or the DAP10ss membioPROTAC described in Figure 3 was introduced by lentivirus. CAR expression levels were assessed by antibody stain for an extracellular tag followed by flow cytometry.

Chapter 6: membioPROTAC abrogates CAR T cell signaling in primary human T cells

We lentivirally transduced primary CD8+ human T cells with a single plasmid encoding the membioPROTAC, CAR and GFP transduction marker separated by 2A elements. To control for the effect of membioPROTAC binding on CAR function, we also engineered T cells with the no degron membioPROTAC negative control.

We challenged anti-CD19 CAR T cells with K562 leukemia cells expressing CD19 or no antigen at a 1:1 effector to target ('E:T') ratio. After 72 hours of co-culture, we measured CAR T cell cytotoxicity, CAR and CD25 expression via flow cytometry. In concordance with data collected in Jurkat cells, membioPROTAC degrades over 99% of detectable CAR in primary T cells. (Fig 8A). This level of membioPROTAC mediated CAR degradation translated to a 60% reduction in target lysis when compared to CAR T cells co-expressing the no degron control (Fig 8B). membioPROTAC mediated degradation of CAR also resulted in a 71% decrease in CD25+ engineered T cells relative to the no degron control and only a 10% increase of CD25+ cells relative to untransduced primary human T cells (Fig 8C). These results suggest that the membioPROTAC can achieve a functionally relevant level of CAR degradation.

Following these results, we explored how the membioPROTAC affects CAR induced cytotoxicity and CAR T cell population levels over time by utilizing a previously published model of mCherry expression Nalm6 acute lymphoblastic leukemia cells[38]. We increased the E:T ratio for these experiments to 3:1 to understand the extent of CAR signaling repression via the membioPROTAC in an overwhelming excess of T cells to tumor cells. We measured Nalm6 populations in these co-culture conditions by live cell fluorescence imaging of mCherry every 3 hours for 72 hours. Gratifyingly, membioPROTAC co-expressing CAR T cells exhibited no

cytotoxicity against Nalm6 cells and behaved similarly to untransduced T cells. By contrast, CAR T cells co-expressing the no degron control exhibited 95% lysis of the Nalm6 population within 24 hours relative to the initial time point (Fig 8D).

We simultaneously tracked CAR T cell populations by quantifying GFP fluorescence levels using live cell fluorescence imaging for 72 hours. CAR T cell cells co-expressing the membioPROTAC demonstrated no proliferation relative to the initial time point, whereas the no degron control expressing CAR T cells showed a 2.4-fold increase in CAR T cell numbers over the course of the experiment (Fig 8E). Together, these data demonstrate that the membioPROTAC functionally abrogates multiple facets of CAR signaling in primary T cells. We observed similar membioPROTAC-dependent suppression of the anti-HER2 CAR, suggesting that membioPROTAC-mediated knockdown may be a generally effective strategy for inhibiting CAR signaling (Fig 9).

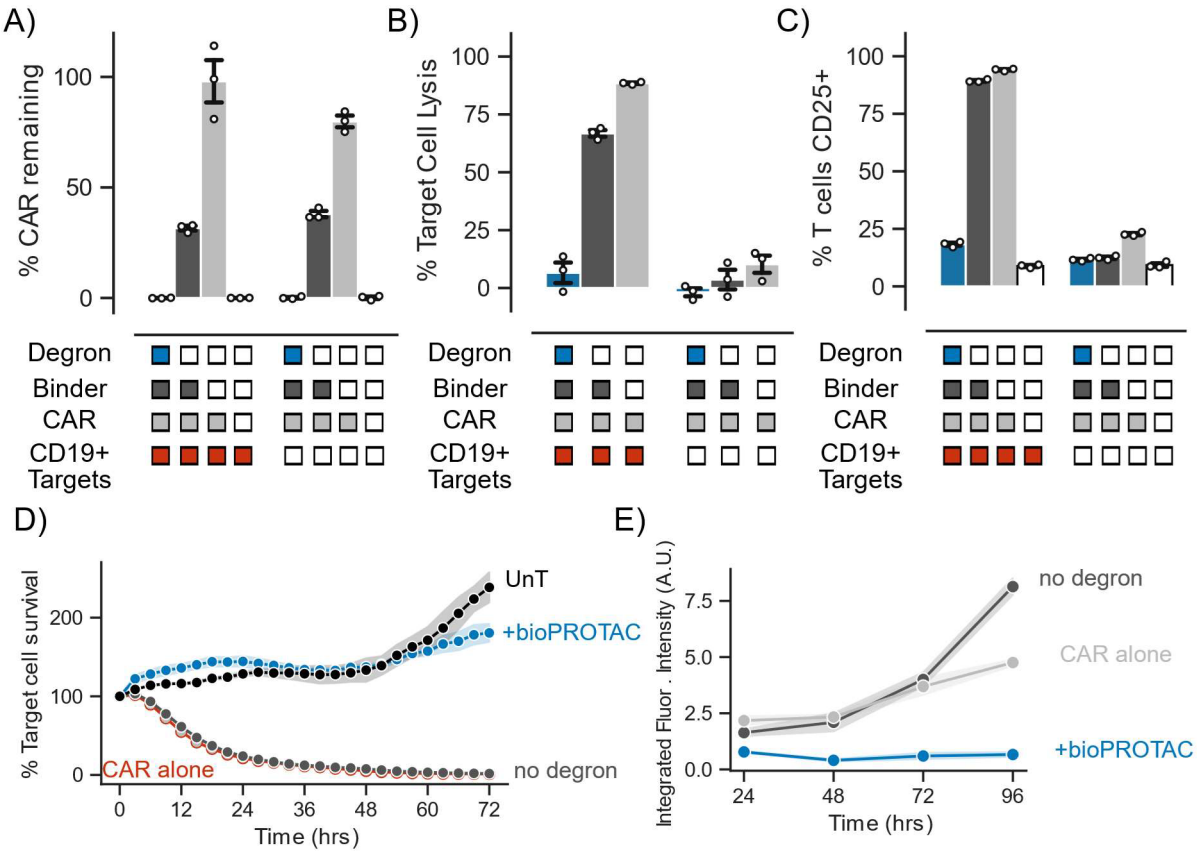

Figure 8. MembioPROTAC abrogated multiple facets of second-generation CAR signaling in primary T cells. (A) membioPROTAC co-expression reduced CAR expression in primary T cells. We assessed degradation efficacy of the membioPROTAC by calculating '% CAR remaining'. % CAR remaining is background subtracted measured CAR fluorescence normalized to the CAR only control. Dots represent technical replicates and error shows SEM. (B) membioPROTAC expression completely abrogated CAR cytotoxicity. Using flow cytometry, we measured CAR T cell cytotoxicity in a 1:1 E:T ratio using CD19 expressing K562s. Dots represent technical replicates and error shows SEM. (C) membioPROTAC prevented upregulation of T cell activation marker CD25. We corroborated functional knockdown of CAR signaling through expression and upregulation of the T cell activation marker CD25. CD25 levels were assessed by antibody staining for the protein and measured by flow cytometry. Dots represent technical replicates and error shows SEM. (E) membioPROTAC ablated CAR functionality even at high E:T ratios sampling during a 72 hour time course. We used the same engineered T cell lines described above and challenged them with Nalm6 cells, a model for acute lymphoblastic leukemia. We co-cultured these cells at an E:T ratio of 3:1 and assayed for target cell clearance by live cell microscopy. Each dot represents the mean of three technical replicates and error shows SEM. (Figure caption continued on the next page)

(Figure caption continued from the previous page) (F) membioPROTAC also stifled CAR T cell proliferation and survival. In this same assay as described in Figure 4E, we observed T cell population numbers by fluorescence over 72 hours by Incucyte image analysis. Each dot represents the mean of three technical replicates and error shows SEM.

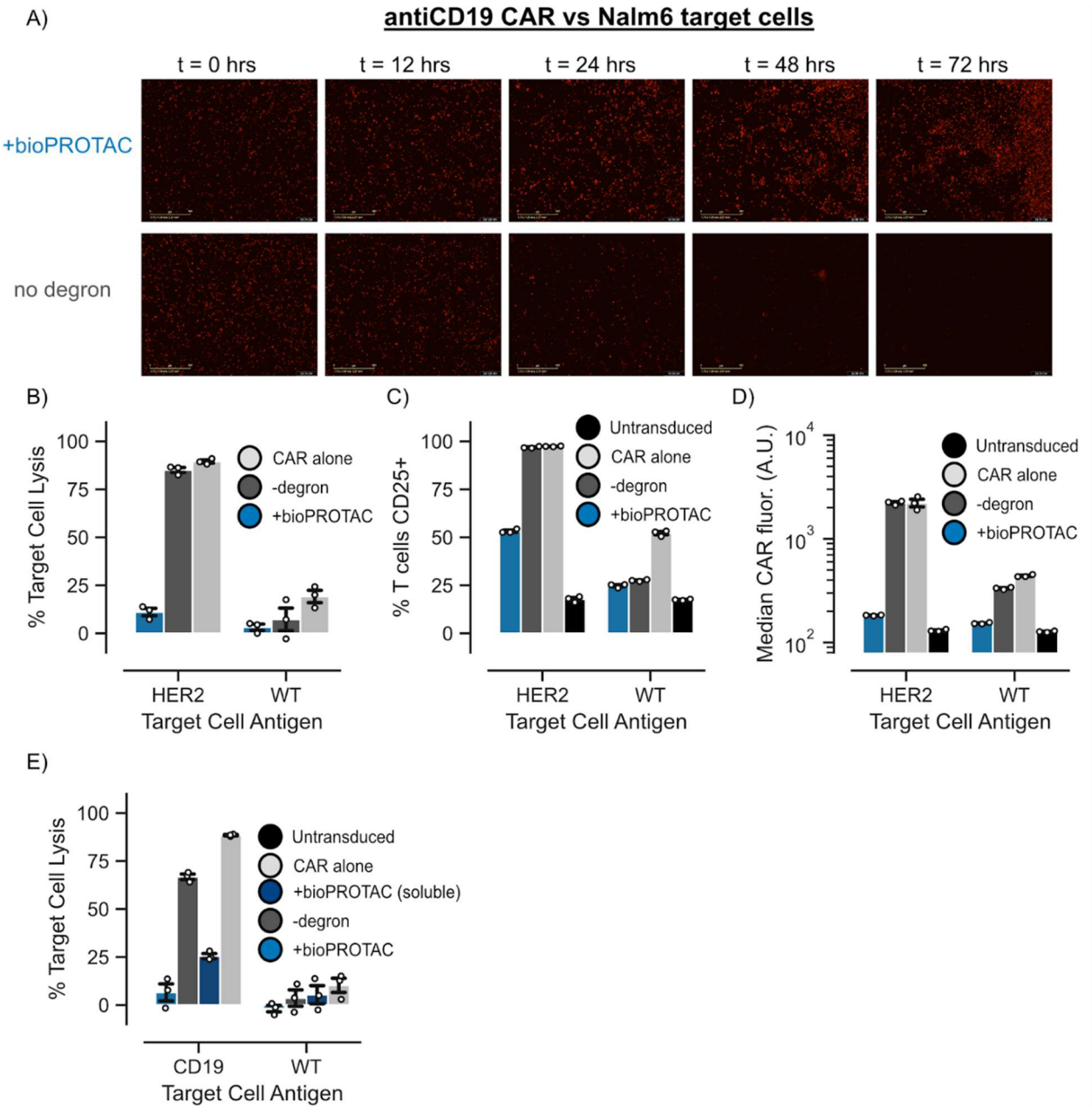

Figure 9. Further characterization of membioPROTAC control of CARs. (A) Representative images of live cell imaging of target cell lysis by CAR T cells. (B-D) membioPROTAC ablated antiHER2 4-1BB CAR activation in primary T cells. CAR T cells were engineered in a similar manner as Figure 4. In these data, CAR T cells target HER2 and K562 cells express HER2 rather than CD19. (E) Membrane localization is required for strong ablation of CAR induced cytotoxicity in primary T cells. Same data as Figure 4A including a control with a cytosolic bioPROTAC.

Chapter 7: bioPROTACs can be compsed into circuits for cell autonomous modulation of CAR T cell signaling

A key characteristic of bioPROTACs is their ability to be genetically encoded. This trait enables the construction of genetic circuits that utilize bioPROTACs to modulate cellular signaling in response to environmental cues and independently of exogenous input such as small molecules. As a proof of concept, we designed a genetic circuit to disrupt T cell signaling upon recognition of a user-defined antigen by targeted degradation of an essential component of the TCR signaling pathway, the tyrosine kinase ZAP70. To enable simultaneous recruitment of the vhhGFP4 nanobody bioPROTAC to ZAP70 and target protein tracking, we adapted a previously published method utilizing CRISPR/Cas9 to tag the N-terminus of endogenous ZAP70 with GFP in primary human CD4+ T cells[36]. We observed that 10% of cells were successfully edited and expressed GFP during isolation by FACS. Following isolation by FACS, 76% of cells retained expression of GFP-ZAP70 (Fig. 10A). We further engineered these T cells via lentiviral transduction of an anti-CD19 4-1BBz CAR, SNIPR responsive to HER2 and a bioPROTAC under the control of a SNIPR responsive promoter. The anti-HER2 SNIPR activates expression of the vhhGFP4 nanobody bioPROTAC in response to the target antigen HER2, which in turn targets the engineered GFP-ZAP70 for degradation to abrogate signaling downstream of the anti-CD19 CAR (Fig 10B). We observed a 47% reduction in GFP+ cells that express the bioPROTAC circuit in the presence of HER2 versus in the absence of HER2 (Fig. 10C).

We designed a repeated challenge assay to explore the effect of the bioPROTAC genetic circuit on engineered CAR T cells over time by measuring GFP-ZAP70 expression, T cell activation, and T cell proliferation and survival after successive rounds of coculture with target

cells (Fig 11D). Considering the time delay between antigen-dependent activation of bioPROTAC expression, degradation of ZAP70, and phenotypic outcomes, we hypothesized that the effect of our circuit may not be evident with a single tumor cell challenge. Indeed, we observed a decrease in GFP-ZAP70 levels, but no difference was observed in CD25 expression or T cell proliferation for engineered T cells cultured with CD19 and HER2 versus CD19 alone target cells after the first challenge (Fig 10E and Fig 11). After a second round of co-culture, we observed a 16% reduction in T cell proliferation and survival for T cells co-cultured with CD19 and HER2 target cells compared to T cells co-cultured with CD19 alone target cells. This difference became more pronounced after a third tumor cell challenge, with bioPROTAC circuit-expressing CAR T cells showing a 45% reduction in proliferation and survival in the presence of HER2 relative to circuit-expressing CAR T cells cultured in the absence of HER2 (Fig. 10E). We also observed that the bioPROTAC circuit reduced CD25 expression by 50% in the presence of the HER2 when compared to CD25 expression of circuit-expressing cells in the absence of HER2 (Fig. 10F). To further validate the role of the bioPROTAC circuit in CAR T cell modulation, we explored how activation of the circuit affected levels of total ZAP70 by intracellular staining. In concordance with the phenotypic data, we observed a 16% reduction in ZAP70+ cells in bioPROTAC circuit expressing cells in the presence of HER2 than in the absence of HER2 (Fig 10G). With these data, we demonstrated that bioPROTACs can be composed into a genetic circuit that uses antigen detection to knockdown a critical protein in T cell activation resulting in changes in CAR T cell phenotypes.

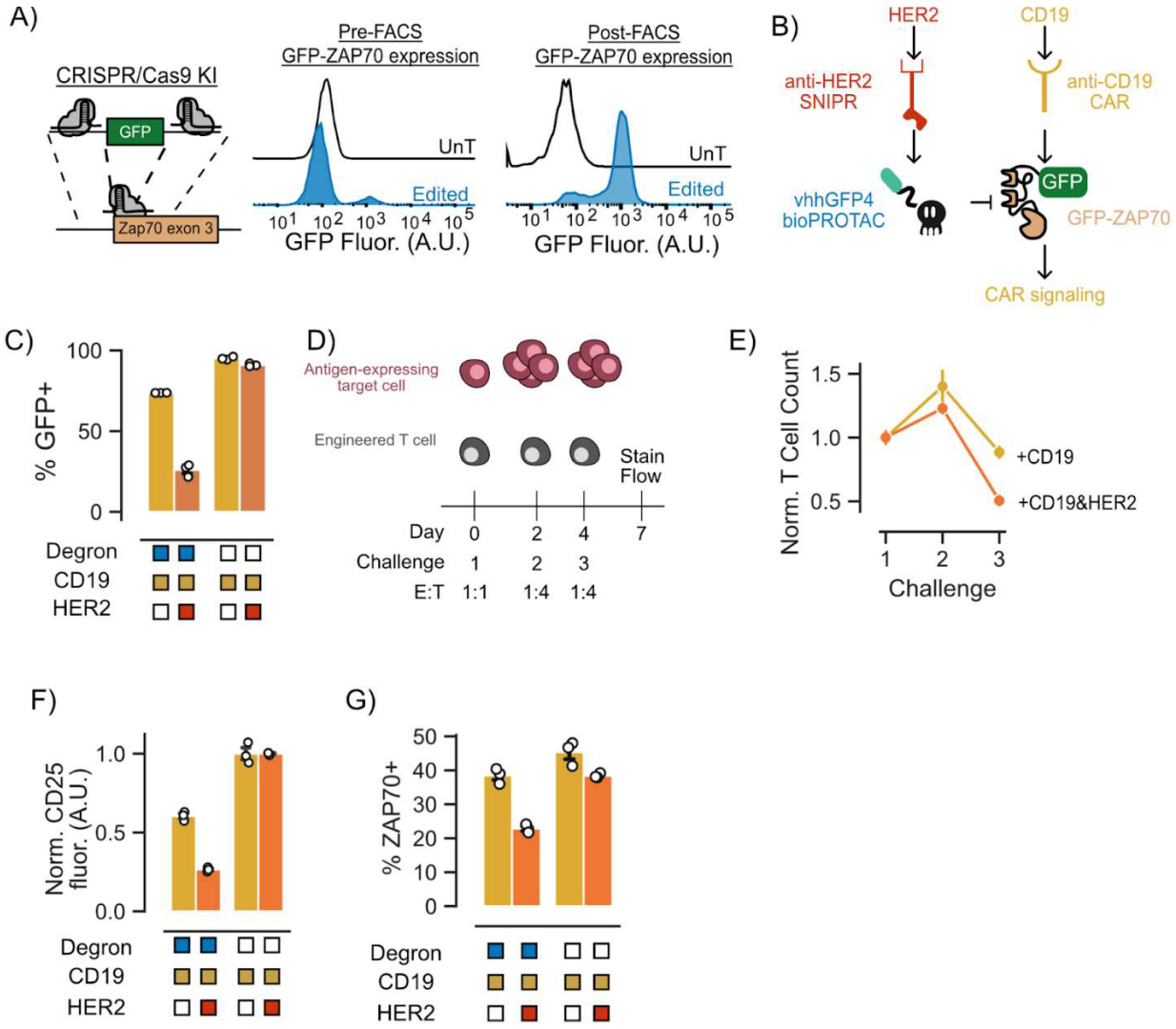

Figure 10. CRISPR/Cas9 knock-in technology can be coupled with bioPROTACs to inducibly degrade endogenous proteins. (A) CRISPR/Cas9 knock-in technology can be used to guide bioPROTACs to endogenous proteins of interest. GFP was knocked into the ZAP70 locus of CD4+ primary T cells to both act as a bioPROTAC recruiting domain and to visualize ZAP70. We observed over 10% of our population expressed GFP-ZAP70 following CRISPR/Cas9 editing. After isolation by FACS, we find that 76% of CD4+ primary T cells retained GFP fluorescence. (B) Cartoon depicting genetic circuit using SNIPR antigen detection to trigger bioPROTAC expression resulting in GFP-ZAP70 degradation. (C) SNIPR-induced bioPROTACs are capable of inducing GFP-ZAP70 degradation as measured by GFP. Alongside CRISPR/Cas9 knock-in, primary CD4+ were additionally engineered with an anti-CD19 4-1BBz CAR and an anti-HER2 SNIPR capable of transcriptionally activating either a vhhGFP4 nanobody bioPROTAC or no degron negative control. (Figure caption continued on the next page.)

(Figure caption continued from the previous page) These cells were then challenged with target cells expressing CD19 or CD19 and HER2 at an E:T ratio of 1:1 for 48 hours. Knockdownof GFP by antigen-induced bioPROTAC activation was measured by flow cytometry. (D) Multiple challenge assay was used to assess circuit functionality. On day 0, engineered T cells were cultured with antigen expressing target cells at an E:T ratio of 1:1. Engineered T cells were rechallenged two more times at an E:T ratio of 1:4. Cell numbers for rechallenge were calculated based on cell counts recovered by flow cytometry. On day 7, the engineered T cell proliferation and survival, CD25 expression and ZAP70 levels were measured by flow cytometry. CD25 levels were ascertained by antibody stain for the protein. ZAP70 levels were ascertained by intracellular staining for total ZAP70. (E) T cell proliferation and survival is also affected by bioPROTAC mediated knockdown of GFP-ZAP70. T cell numbers were quantified using flow cytometry and normalized to the no degron control for each antigen condition. Proliferation and survival were calculated based on the number of T cells recovered by flow cytometry. T cell counts were then normalized to the no degron control and then again normalized to the first challenge. Dots are the mean of three technical replicates and error bars represent SEM. (F) bioPROTAC-mediated knockdown of GFP-ZAP70 resulted in functional consequences in CAR T cell signaling. Following the multi-challenge assay, cells were stained for the activation marker CD25. Each dot on the line represents the mean of three technical replicates. The error shown represents the SEM. CD25 fluorescence values were normalized to those of cells expressing the no degron control circuit. (G) SNIPR-induced bioPROTACs are capable of inducing GFP-ZAP70 degradation as measured by total ZAP70 levels. After a multi-challenge assay, the ZAP70 levels of each cell type was measured by flow cytometry. ZAP70 levels were ascertained by intracellular staining. T cells were isolated from target cells based on staining of CD3. ZAP70+ cells were determined by *in silico* gating. Each dot represents technical replicates and error bars show SEM. ZAP70 fluorescence values were normalized to those of cells expressing the no degron control circuit.

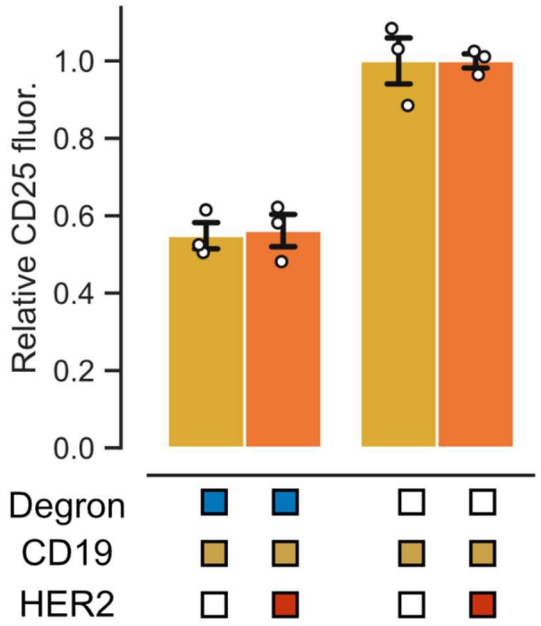

Figure 11. bioPROTAC circuit does not affect CD25 levels following single challenge. We observed no changes in CD25 levels in CAR T cells that express the bioPROTAC circuit when co-cultured with CD19 versus those cultured with CD19+HER2. Dots represent technical triplicates and error bars show SEM. CD25 fluorescence were normalized to those of CAR T cell expressing the no degron control.

Chapter 8: Concluding Remarks

To create an ideal bioPROTAC for T cell engineering, we took a bottom-up approach to develop a novel bioPROTAC drawing inspiration from the endogenous UPS and previously published bioPROTACs. We required that our novel bioPROTAC fulfilled two major requirements: compactness and flexible targeting of POIs. Here, we introduced a bioPROTAC that can be as small as 181 base pairs, making it ideal for retroviral delivery and for use in genetic circuits. We demonstrated bioPROTAC modularity using structurally different and orthogonal protein-protein interaction domains to guide POI binding. This modularity could be used to direct the bioPROTAC against any potential POI and is limited only by the availability of protein-protein interaction domains. With the improvement in antibody fragment development and, especially, the rapidly growing *de novo* designed protein field, the list of possible targeting binding domains continues to grow greatly improving the potential of bioPROTACs. Our lab, in collaboration with the Baker group, recently showed the use of *de novo* designed proteins as antigen recognition domains for synNotch thus it is not beyond imagination that similar methods could be applied to the recruitment of bioPROTACs to any protein of interest[37].

We also found that the bioPROTAC can be tunable through mutagenesis of lysine residues in the binding domain. Interestingly, we found that mutagenesis improved SynZip18 bioPROTAC degradation but had minimal effect on SynZips2 and 17. We hypothesize that this could be attributed to availability of surface lysine residues. Further investigation into how these structurally similar proteins are differentially affected by this mutagenesis could be an interesting

avenue for optimization of future bioPROTAC designs and to gain a better understanding of the mechanisms behind cis-ubiquitylation.

Another useful property of our bioPROTAC is its robust degradation across many mammalian cell types. While engineered T cells are immensely successful in the clinic, other engineered cell types have shown great promise as therapeutic cell chassis. We show that the bioPROTAC can be used in classic cell engineering cell lines, such as HEK293T cells, which can be useful for prototyping potential circuit architectures and guiding foundational cell engineering principles. We also show that the bioPROTAC is an effective degrader in mESCs which can be used to guide exploratory discoveries in fields such as developmental biology. Some cell types of interest that we did not show, but could benefit from the principles shown in this work are human stem cells, natural killer (NK) cells and macrophages. Induced pluripotent stem cells are promising chassis cells with many promising applications in drug discovery, disease modeling and cell therapies[38]. CAR NK cells are a promising branch of CAR immunotherapies due to their potent cytotoxicity and lower observed frequency of patient toxicity[39]. CAR macrophages offer an alternative mode of tumor clearance that also augments native T cell activity[40,41]. The implementation of bioPROTAC technology alone or composed into genetic circuits could benefit future cell engineering in a variety of mammalian cell types.

Upon investigation into the mechanism of bioPROTAC mediated degradation, we identified cullin ring ligase as a major player in the degradation of both cytosolic and membrane proteins. We showed that bioPROTAC degradation relies on the proteasome for cytosolic protein targets. However, bioPROTAC-based degradation of membrane protein targets is not influenced

by the proteasome. However, unlike other tools, such as LYTACS and AbTACs, our data did not implicate the lysosome in the degradation of membrane proteins[20,42]. Further investigation into the mechanism of bioPROTAC mediated degradation of membrane proteins could elucidate some unexpected degradation pathways. Furthermore, we used dominant negative cullins to identify the CUL4A and 4B families as mediators for bioPROTAC degradation. Interestingly, perturbation of the CUL2 family did not have an observable effect. This does not completely align with previously described rules of C-terminal degron degradation of the mammalian proteome. We hypothesize that this discordance may hint at the preference of cullin families amongst different cell lines.

Characterization of bioPROTAC degradation revealed that titration of bioPROTAC expression levels results in dose-dependent degradation. We also observed that bioPROTAC degradation occurred as early as 4 hours post doxycycline induction. This degradation rate rivals that of previously published bioPROTACs tools. This rapid degradation is also seen in our SNIPR-based circuit where transcriptional activation of the bioPROTAC still results in over 75% of target protein degradation within 48 hours. This understanding of bioPROTAC kinetics can aid in *in silico* modeling of potential bioPROTAC circuits thereby narrowing the searchable space of bioPROTAC applications.

Our bioPROTAC uses intracellular protein-protein interactions to guide TPD while other tools rely on the administration of a soluble extracellular factor to aid in degradation. While this secondary molecule provides additional control over TPD, we opted for the use of genetic circuits as our method of control instead. These genetic circuits allow for cell-by-cell logic

processing to interpret environmental cues for appropriate cellular actions. Here, we devised a circuit that uses CRISPR/Cas9 to edit the endogenous ZAP70 locus to mark the protein for degradation and SNIPR to use environmental cues to drive bioPROTAC activation. While this circuit was successful by some metrics, further optimization is necessary for its implementation as a therapeutic strategy. We found that even after multiple challenges, bioPROTAC degradation was insufficient to ablate target cell lysis (data not shown). We hypothesize that this could be due to CAR signaling through non-ZAP70 mediated pathways. Direct degradation of the CAR using bioPROTACs could potentially circumvent this issue. However, our attempts at a circuit that uses SNIPRs to induce expression of a bioPROTAC to degrade a CAR were unsuccessful. We hypothesize that this inability to regulate the CAR is due to inability to produce a sufficient level of bioPROTAC within a therapeutically relevant time frame. The use of post-translational methods to activate the bioPROTAC could vastly improve the kinetics of degradation. Alternatively, we could target multiple constituents of the TCR pathway using similar CRISPR/Cas9 methods using pairs of orthogonal binders shown in this work.

The circuit in its current state is unable to be used in therapeutic applications. However, it is a powerful proof of concept demonstrating the potential of implementing cell autonomous control of CAR T cell signaling using protein degradation. In this work, we show that bioPROTACs can be transcriptionally activated by the proteolytic receptor SNIPR. We postulate that bioPROTACs, as a completely protein-based tool, could be coupled with existing technologies to dictate bioPROTACs expression, function, and localization [44–46]. We highlighted this property of bioPROTACs by replacing the transcriptional activation domain of SNIPRs with

the bioPROTAC. We demonstrated a moderate effect of antigen-dependent POI degradation (Figure S5). While the potency of degradation falls short of expectations, further optimization of this design could result in quicker degradation. Additionally, we demonstrated that bioPROTACs can be integrated into endogenous signaling networks to modulate cell signaling. This is beneficial for both clinical and discovery scientific applications.

While we show a simple proof-of-concept antigen-based degradation circuit here, the potential for novel circuits is limitless. For example, we postulate that bioPROTACs can be used in a negative feedback circuit using previously published CAR response elements to recapitulate the findings that dynamic CAR regulation is a key component of combating T cell exhaustion[43]. These dynamic regulatory circuits could be vital in the development of next-generation CAR T cells capable of cell autonomous and reactive regulation of CAR signaling.

Genetic circuits that endow cell autonomous control over therapeutic functions could greatly improve the safety, specificity and efficacy of engineered cell therapies. Targeted protein degradation perfectly complements current approaches in genetic circuit design and implementation and is a highly effective method for modulating signaling. We believe that the bioPROTAC developed in this work could be useful for many future cell engineering endeavors.

Chapter 9: Material and Methods

Gene synthesis and cloning:

All plasmids were cloned using the Mammalian Toolkit ('MTK'), a Golden-Gate based cloning system[44]. All parts plasmids from the MTK used in this work were domesticated from DNA sequences generated by oligonucleotide annealing, gBlocks or PCR. SNIPR plasmids were domesticated by PCR using plasmids gifted by Dr. Kole Roybal as a template. Plasmids synthesized in this manner were propagated in Stbl3 *E. coli* from QB3 Macrolab. All part plasmids were verified by sequencing and all subsequent plasmids were verified by test restriction digest and sequencing.

Jurkat T cell culture conditions:

Jurkat T cells were cultured in RPMI-1640 (Gibco #11875-093) supplemented with 10% fetal bovine serum (FBS) and 1% anti-anti (Gibco #15240-096). Cells were maintained in T75 flasks and split 1:10 every 3 days.

K562 target cell generation and cell culture conditions:

K562 target cells expressing CD19, HER2 or CD19&HER2 were generated by lentiviral transduction using plasmids gifted by Dr. Wendell Lim and his lab. K562s were cultured in IMDM supplemented with 10% FBS and 1% gentamicin. K562 cells were maintained in T25 flasks and split 1:10 every 3 days.

Source of primary human T cells:

Blood was obtained from Blood Centers of the Pacific (San Francisco, CA) as approved by the University Institutional Review Board. Primary CD4+ and CD8+ T cells were isolated from anonymous donor blood after apheresis as described below.

Primary human T cell isolation:

Primary CD4+ and CD8+ T cells were isolated from anonymous donor blood after apheresis by negative selection. T cells were cryo-preserved in CellBanker cell freezing media.

Cell culture for Lenti-X 293T cells:

Lenti-X 293T packaging cells (Clontech #11131D) were cultured in medium consisting of Dulbecco's Modified Eagle Medium (DMEM) (Gibco #10569-010) and 10% fetal bovine serum (FBS) (University of California, San Francisco ('UCSF') Cell Culture Facility). Lenti-X 293T cells were cultured in T150 or T225 flasks (Corning #430825 and #431082) and passaged upon reaching 80% confluency. To passage, cells were treated with TrypLE express (Gibco #12605010) at 37 C for 5 minutes. Then, 10 mL of media was used to quench the reaction and cells were collected into a 50 mL conical tube and pelleted by centrifugation (400xg for 4 minutes). Cells were cultured until passage 30 whereupon fresh Lenti-X 293 T cells were thawed.

Cell culture for HEK 293T cells:

HEK 293T cells (UCSF Cell Culture Facility) were cultured in medium consisting of Dulbecco's Modified Eagle Medium (DMEM) (Gibco #10569-010) and 10% fetal bovine serum (FBS) (UCSF Cell Culture Facility). HEK 293T cells were cultured in T75 flasks (Corning #430641U) and passaged upon reaching 80% confluency.

Cell culture for 3T3 cells:

3T3 cells were cultured in medium consisting of Dulbecco's Modified Eagle Medium (DMEM) (Gibco #10569-010) and 10% fetal bovine serum (FBS) (UCSF Cell Culture Facility). 3T3 cells were passaged upon reaching 80% confluency. To pass, cells were treated with TrypLE express at 37 C for 3 minutes. Then, 10 mL of media was added to quench the reaction and cells were collected into a 50 mL conical tube and pelleted by centrifugation (400xg for 4 minutes). Pellet was resuspended in 5 mL and 1 mL of resuspended pellet was added to a T25 flask (Corning #430639) containing 10 mL of media.

Culture of mouse embryonic stem cells (mESCs):

mESCs were cultured in "Serum Free ES" (SFES) media supplemented with 2i. SFES media consists of 500 mL DMEM/F12 (Gibco #11320-033), 500 mL Neurobasal (Gibco #21103-049), 5 mL N2 Supplement (Gibco #17502-048), 10 mL B27 with retinoic acid (gibco #17504-044), 6.66 mL 7.5% BSA (Gibco #15260-037), 10 mL 100x GlutaMax (Gibco #35050-061), and 10 mL 100x Pen/Strep. To make "2i SFES" media, 1 nM PD03259010 (Selleckchem #S1036), 3

nM CHIR99021 (Selleckchem #S2924) and 1000 units/mL LIF (ESGRO #ESG1106) were added to 45 mL SFES. Prior to use, 1-thioglycerol (MTG; Sigma M6145) was diluted 1.26% in SFES and added 1:1000 to 2i SFES media. To passage, mESCs were treated with 1 mL of accutase in a 6 well plate (Corning #353046) for 5 minutes at room temperature (RT). After incubation, cells were mixed by pipette and moved to a 15 mL conical tube, supplemented with 10 mL SFES and spun at 300xg for 3 minutes. Then, media was removed and cells were counted using the Countess II Cell Counter (ThermoFisher) according to the manufacturer's instructions. Cells were then plated in 6 well plates that had gelatinized with 1% gelatin for 30 minutes at 37 C at 5 x 10^5 cells per well in 2 mL of 2i SFES. Media was changed every day and cells were split every other day. Cells and culturing reagents were gifted by Dr. Abby Buchwalter.

Primary Human T Cell Isolation and Culture:

After thawing, T cells were cultured in human T cell medium (hTCM) consisting of X-VIVO 15 (Lonza #04-418Q), 5% Human AB serum and 10 mM neutralized N-acetyl L-Cysteine (Sigma-Aldrich #A9165) supplemented with 30 units/mL IL-2 (NCI BRB Preclinical Repository) for all experiments.

Lentiviral transduction of primary T cells using LentiX concentrator:

Pantropic VSV-G pseudotyped lentivirus was produced via transfection of Lenti-X 293T cells with a modified pHR'SIN:CSW transgene expression vector and the viral packaging plasmids

pCMVdR8.91 and pMD2.G using Fugene HD (Promega #E2312). Primary T cells were thawed the same day, and after 24 hr in culture, were stimulated with Dynabeads Human T-Activator CD3/CD28 (Thermo Scientific #11131D) at a 1:3 cell:bead ratio. At 48 hr, viral supernatant was harvested and concentrated using the Lenti-X concentrator (Takara, #631231) according to the manufacturer's instructions. Briefly, viral supernatant was harvested and potential contaminants were filtered using a 0.45 μM filter (Millipore Sigma #SLHV033RS). Lenti-X concentrator solution was added at a 1:3 viral supernatant:concentrator ratio, mixed by inversion, and incubated at 4 C for at least 2 hours. Supernatant-concentrator mix was pelleted by centrifugation at 1500xg at 4 C for 45 minutes, supernatant was removed and pellet was resuspended using 100 μL media or PBS (UCSF Cell Culture Facility) for each well of T cells. Typically, 2 wells of a 6 well plate was concentrated for 1 well of a 24 well plate plated with 1 million T cells on day of transfection. The primary T cells were exposed to the virus for 24 hours and viral supernatant was exchanged for fresh hTCM supplemented with IL-2 as described above. At day 5 post T cell stimulation, Dynabeads were removed and the T cells expanded until day 12-14 when they were rested for use in assays. For co-culture assays, T cells were sorted using a Sony SH-800 cell or BD FACS Aria sorter on day 5-6 post stimulation.

Flow cytometry:

All flow cytometry data was obtained using a LSR Fortessa or LSRII (BD Biosciences). All assays were run in a 96-well round bottom plate (Fisher Scientific #08-772-2C). Samples were prepared by pelleting cells in the plate using centrifugation at 400xg for 4 minutes. Supernatant

was then removed and 200 µL of PBS (UCSF Cell Culture facility) was used to wash cells. The cells were again pelleted as described above and supernatant was removed. Cells were resuspended in flow buffer (PBS + 2% FBS) and mixed by pipetting prior to flow cytometry assay.

Inhibitor Assays:

100,000 cells were plated in a 96 well round bottom plate with either 5 µM MG-132 (Sigma-Aldrich #M7449-200UL), 1 µM MLN4924(Active Biochem #A-1139), 100 nM Bafilomycin A1(Enzo Life Sciences #BML-CM110-0100), or DMSO vehicle control and incubated at 37 C for 5 hours. After incubation, cells were pelleted by centrifugation at 400xg for 4 minutes. Supernatant was then removed and cells were washed once with 200 µL PBS. Cells were pelleted again (400xg for 4 minutes) and resuspended in flow buffer (PBS + 2% FBS) for assay by flow cytometry.

Antibody staining:

All experiments using antibody staining were performed in 96 well round bottom plates. Cells for these assays were pelleted by centrifugation (400xg for 4 minutes) and supernatant was removed. Cells were washed once with 200 µL of PBS and pelleted again by centrifugation (400xg for 4 minutes) and the supernatant was removed. Cells were resuspended in a staining solution of 50 µL PBS containing fluorescent antibody stains of interest. Anti-myc antibodies (Cell Signaling Technologies #2233S, #3739S and #2279S) was used at a 1:100 ratio while

antiV5 (ThermoFisher Scientific #12-679642) and antiFLAG (R&D Systems #IC8529G-100) antibodies were used at a 1:50 ratio for flow cytometry assays. For FACS, all antibodies were used in a 1:50 ratio in 100 uL.

Intracellular staining:

For intracellular staining assays, cells were pelleted at 400xg for 4 minutes following co-culture. After careful remove of supernatant by, cells were treated with Zombie UV fixable Viability kit diluted 1:500 in PBS for 30 minutes in the dark at room temperature. Cells then underwent fixation and permeabilization using an eBiosciences Foxp3/Transcription Factor Staining Buffer Set (ThermoFisher #00-5523-00) following manufacturer's recommended procedure. Prior to fixation, Following the fixation/permeabilization process, cells were stained with Zap-70 (136F12) Rabbit mAb (PE Conjugate) (Cell Signaling #93339) for 1 hour at room temperature in the dark. The stain was then washed off with the perm/wash buffer in the eBiosciences kit twice and resuspended in flow buffer. Cells were the analyzed by flow cytometry.

CRISPR/Cas9 HDR knock-in template generation:

CRISPR/Cas9 knock-in template was generated using PCR from a plasmid encoding the homology arms and desired knock-in payload as described in Shy et al. Double-stranded DNA was purified by solid phase reversible immobilization (SPRI) bead cleanup using AMPure XP beads (Beckman Coulter #A63881). Beads were added in 1.8:1 volume:volume ratio to PCR template and isolated per manufacturer's instructions. For GFP-ZAP70 template, HDR template

was eluted in 30 µL of water.

CRISPR/Cas9 RNP formulation

RNPs were produced following protocols described in Shy et al. crRNA and tracRNA were synthesized by IDT and resuspended in provided buffer at 160 µM and kept as 3 µL aliquots at -80 C. All incubation steps described in this section were performed on a heat block. gRNA was made by mixing crRNA and tracrRNA at 1:1 v/v ratio and annealed by incubation for 20 minutes at 37 C. ssDNAenh (IDT) was added at 0.8:1 v/v ratio and mixed by pipette. The ssDNAenh electroporation enhancer is a sequence described by Shy et al. shown to improve knock-in efficiency. The ssDNAenh (5'-TCATGTGGTCGGGGTAGCGGCTGAAGCACTGCACGCCGTACGTCAGGGTGGTCACGAGGGTGGGCCAGGGCACGGGCAGCTTGCCGGTGGTGCAGATGAACTTCAGGGTCAGCTTGCCGTAGGTGGC-3') was synthesized by IDT, resuspended to 100 µM in duplex buffer and stored at −80 °C in 5 µL aliquots. Then, 40 µM of Cas9-NLS (Berkeley QB3 Macrolab) was added to the gRNA+ssDNAenh mixture at a 1:1 v/v ratio. This results in a final molar ratio of sgRNA:Cas9 of 2:1. This mixture was mixed by pipette and incubated for 15 minutes at 37 C. Based on a Cas9 protein basis, 50 pmol of RNP was used for each electroporation.

Electroporation:

Electroporation was done 7 days after stimulation by DynaBeads using a P3 Primary Cell 4D-Nucleofector™ X Kit (Lonza #V4XP-3012). 750 ng of HDR template was mixed with 50 pmol

of RNP and incubated at room temperature for 10 minutes. During this incubation, DynaBeads were removed from cells and cells were spun at 200xg for 7 minutes. Supernatant was removed and cells were resuspended in 20 µL of Lonza P3 buffer. RNP+HDR template mixture was added to cells and 20 µL of this mixture was then added to electroporation vessel. Cells were then electroporated using a Lonza 4D-Nucleofector® X Unit (Lonza #AAF-1003X) with code EH-115. Immediately, 90 µL of warm hTCM+IL-2 was added to cells and cells were then incubated for 20 minutes at 37 C. Cells were then transferred to a fresh 96 well plate and diluted to 1.0×10^6 cells per ml in hTCM+IL-2 and 0.05 µM of the small molecule inhibitor TSA (Cayman Chemical). The 96 well plate was then spun at 200xg for 7 min and incubated in a tissue culture incubator overnight. 24 hours following TSA treatment, TSA-containing media was removed and fresh hTCM+IL-2 was added. Fresh cytokines and media were added every 2-3 days until sorting by FACS.

Co-culture assays:

For all assays, T cells and target cells were co-cultured at a specified effector to target ratios with cell numbers varying per assay. All assays contained between 10,000 and 50,000 of each cell type. The Countess II Cell Counter (ThermoFisher) was used to determine cell counts for all assays set up. T cells and target cells were mixed in 96-well round bottom tissue culture plates in 200 µL T cell media, and then plates were centrifuged for 1 min at 400x g to initiate interaction of the cells prior to incubation at 37 C.

Incucyte cell lysis assays:

Primary human CD8+ T cells and target cells were plated in a flat bottom 96 well plates (cat num.). For suspension target cells, wells were coated with 50 µL of 5 µg/mL fibronection and incubated for 1 hour at room temperature. Fibronectin solution was then removed and plates were left to dry in a biosafety cabinet for 1 hour. Engineered T cells and target cells are then added at effector:target ratios as needed and allowed to settle at room temperature for 30 minutes. Images were taken every 3 hours using Incucyte hardware and software over the course of the experiments.

Data analysis:

Data analysis was performed using the FlowJo software (FlowJo LLC.) and Python. For co-culture assays, desired cell populations were isolated by FACS using a Sony SH800 or Aria (BD) cell sorter. For non co-culture assays, desired cell populations were isolated by gating in FlowJo following flow cytometry. Incucyte data was analyzed and quantified by Incucyte software and plotted using Python.

References:

1. Elowitz, M. B. & Leibler, S. A synthetic oscillatory network of transcriptional regulators. *Nature* **403**, 335–338 (2000).
2. Gardner, T. S., Cantor, C. R. & Collins, J. J. Construction of a genetic toggle switch in Escherichia coli. *Nature* **403**, 339–342 (2000).
3. June, C. H. & Sadelain, M. Chimeric Antigen Receptor Therapy. *N. Engl. J. Med.* **379**, 64–73 (2018).
4. Cappell, K. M. & Kochenderfer, J. N. Long-term outcomes following CAR T cell therapy: what we know so far. *Nat. Rev. Clin. Oncol.* **20**, 359–371 (2023).
5. Brown, C. E. & Mackall, C. L. CAR T cell therapy: inroads to response and resistance. *Nat. Rev. Immunol.* **19**, 73–74 (2019).
6. Lim, W. A. & June, C. H. The Principles of Engineering Immune Cells to Treat Cancer. *Cell* **168**, 724–740 (2017).
7. Morsut, L. *et al.* Engineering Customized Cell Sensing and Response Behaviors Using Synthetic Notch Receptors. *Cell* **164**, 780–791 (2016).
8. Roybal, K. T. *et al.* Precision Tumor Recognition by T Cells With Combinatorial Antigen-Sensing Circuits. *Cell* **164**, 770–779 (2016).
9. Zhu, I. *et al.* Modular design of synthetic receptors for programmed gene regulation in cell therapies. *Cell* **185**, 1431–1443.e16 (2022).
10. Choe, J. H. *et al.* SynNotch-CAR T cells overcome challenges of specificity, heterogeneity, and persistence in treating glioblastoma. *Sci. Transl. Med.* **13**, eabe7378 (2021).

11. Williams, J. Z. *et al.* Precise T cell recognition programs designed by transcriptionally linking multiple receptors. *Science* **370**, 1099–1104 (2020).
12. Hyrenius-Wittsten, A. *et al.* SynNotch CAR circuits enhance solid tumor recognition and promote persistent antitumor activity in mouse models. *Sci. Transl. Med.* **13**, (2021).
13. Allen, G. M. *et al.* Synthetic cytokine circuits that drive T cells into immune-excluded tumors. *Science* **378**, eaba1624 (2022).
14. Hyrenius-Wittsten, A. & Roybal, K. T. Paving New Roads for CARs. *Trends Cancer Res.* **5**, 583–592 (2019).
15. Weber, E. W. *et al.* Pharmacologic control of CAR-T cell function using dasatinib. *Blood Advances* **3**, 711–717 (2019).
16. Burslem, G. M. *et al.* The Advantages of Targeted Protein Degradation Over Inhibition: An RTK Case Study. *Cell Chemical Biology* **25**, 67–77.e3 (2018).
17. Carbonneau, S. *et al.* An IMiD-inducible degron provides reversible regulation for chimeric antigen receptor expression and activity. *Cell Chemical Biology* (2020) doi:10.1016/j.chembiol.2020.11.012.
18. Jan, M. *et al.* Reversible ON- and OFF-switch chimeric antigen receptors controlled by lenalidomide. *Sci. Transl. Med.* **13**, eabb6295 (2021).
19. Weber, E. W. *et al.* Transient rest restores functionality in exhausted CAR-T cells through epigenetic remodeling. *Science* **372**, eaba1786 (2021).

20. Portnoff, A. D., Stephens, E. A., Varner, J. D. & DeLisa, M. P. Ubiquibodies, Synthetic E3 Ubiquitin Ligases Endowed with Unnatural Substrate Specificity for Targeted Protein Silencing. *J. Biol. Chem.* **289**, 7844–7855 (2014).

21. Zhao, W., Pferdehirt, L. & Segatori, L. Quantitatively Predictable Control of Cellular Protein Levels through Proteasomal Degradation. *ACS Synth. Biol.* **7**, 540–552 (2018).

22. Zhao, L., Zhao, J., Zhong, K., Tong, A. & Jia, D. Targeted protein degradation: mechanisms, strategies and application. *Signal Transduction and Targeted Therapy* **7**, 113 (2022).

23. Cotton, A. D., Nguyen, D. P., Gramespacher, J. A., Seiple, I. B. & Wells, J. A. Development of Antibody-Based PROTACs for the Degradation of the Cell-Surface Immune Checkpoint Protein PD-L1. *J. Am. Chem. Soc.* (2021) doi:10.1021/jacs.0c10008.

24. Caussinus, E., Kanca, O. & Affolter, M. Fluorescent fusion protein knockout mediated by anti-GFP nanobody. *Nat. Struct. Mol. Biol.* **19**, 117–121 (2012).

25. Prozzillo, Y. *et al.* Targeted Protein Degradation Tools: Overview and Future Perspectives. *Biology* **9**, 421 (2020).

26. Canté-Barrett, K. *et al.* Lentiviral gene transfer into human and murine hematopoietic stem cells: size matters. *BMC Res. Notes* **9**, 1–6 (2016).

27. Bonger, K. M., Chen, L.-C., Liu, C. W. & Wandless, T. J. Small-molecule displacement of a cryptic degron causes conditional protein degradation. *Nat. Chem. Biol.* **7**, 531–537 (2011).

28. Melvin, A. T. *et al.* A Comparative Analysis of the Ubiquitination Kinetics of Multiple Degrons to Identify an Ideal Targeting Sequence for a Proteasome Reporter. *PLoS One* **8**, e78082 (2013).

29. Fan, X., Jin, W. Y., Lu, J., Wang, J. & Wang, Y. T. Rapid and reversible knockdown of endogenous proteins by peptide-directed lysosomal degradation. *Nat. Neurosci.* **17**, 471–480 (2014).

30. Melvin, A. T., Dumberger, L. D., Woss, G. S., Waters, M. L. & Allbritton, N. L. Identification of a p53-based portable degron based on the MDM2-p53 binding region. *Analyst* **141**, 570–578 (2016).

31. Thompson, K. E., Bashor, C. J., Lim, W. A. & Keating, A. E. SYNZIP Protein Interaction Toolbox: in Vitro and in Vivo Specifications of Heterospecific Coiled-Coil Interaction Domains. *ACS Synth. Biol.* **1**, 118–129 (2012).

32. Kirchhofer, A. *et al.* Modulation of protein properties in living cells using nanobodies. *Nat. Struct. Mol. Biol.* **17**, 133–138 (2010).

33. Daniel, K. *et al.* Conditional control of fluorescent protein degradation by an auxin-dependent nanobody. *Nat. Commun.* **9**, 3297 (2018).

34. Koren, I. *et al.* The Eukaryotic Proteome Is Shaped by E3 Ubiquitin Ligases Targeting C-Terminal Degrons. *Cell* **173**, 1622–1635.e14 (2018).

35. Hernandez-Lopez, R. A. *et al.* T cell circuits that sense antigen density with an ultrasensitive threshold. *Science* **371**, 1166–1171 (2021).

36. Wu, C.-Y., Roybal, K. T., Puchner, E. M., Onuffer, J. & Lim, W. A. Remote control of therapeutic T cells through a small molecule–gated chimeric receptor. *Science* **350**, aab4077 (2015).

37. Arai, R., Ueda, H., Kitayama, A., Kamiya, N. & Nagamune, T. Design of the linkers which effectively separate domains of a bifunctional fusion protein. *Protein Eng. Des. Sel.* **14**, 529–532 (2001).

38. Majzner, R. G. *et al.* Tuning the Antigen Density Requirement for CAR T-cell Activity. *Cancer Discov.* **10**, 702–723 (2020).

39. Shy, B. R. *et al.* High-yield genome engineering in primary cells using a hybrid ssDNA repair template and small-molecule cocktails. *Nat. Biotechnol.* **41**, 521–531 (2023).

40. Banik, S. M. *et al.* Lysosome-targeting chimaeras for degradation of extracellular proteins. *Nature* 1–7 (2020).

41. Myers, J. A. & Miller, J. S. Exploring the NK cell platform for cancer immunotherapy. *Nat. Rev. Clin. Oncol.* **18**, 85–100 (2020).

42. Weinberg, Z. Y. *et al.* Sentinel cells enable genetic detection of SARS-CoV-2 Spike protein. *bioRxiv* (2021) doi:10.1101/2021.04.20.440678.

43. Eyquem, J. *et al.* Targeting a CAR to the TRAC locus with CRISPR/Cas9 enhances tumour rejection. *Nature* **543**, 113–117 (2017).

44. Gao, X. J., Chong, L. S., Kim, M. S. & Elowitz, M. B. Programmable protein circuits in living cells. *Science* **361**, 1252–1258 (2018).

45. Vlahos, A. E. *et al.* Protease-controlled secretion and display of intercellular signals. *bioRxiv* 2021.10.18.464444 (2021).

46. Chen, Z. & Elowitz, M. B. Programmable protein circuit design. *Cell* (2021) doi:10.1016/j.cell.2021.03.007.

47. Fonseca, J. P. *et al.* A Toolkit for Rapid Modular Construction of Biological Circuits in Mammalian Cells. *ACS Synth. Biol.* **8**, 2593–2606 (2019).

Publishing Agreement

It is the policy of the University to encourage open access and broad distribution of all theses, dissertations, and manuscripts. The Graduate Division will facilitate the distribution of UCSF theses, dissertations, and manuscripts to the UCSF Library for open access and distribution. UCSF will make such theses, dissertations, and manuscripts accessible to the public and will take reasonable steps to preserve these works in perpetuity.

I hereby grant the non-exclusive, perpetual right to The Regents of the University of California to reproduce, publicly display, distribute, preserve, and publish copies of my thesis, dissertation, or manuscript in any form or media, now existing or later derived, including access online for teaching, research, and public service purposes.

DocuSigned by:
Matthew Kim
7CF05E83F84C4F0...
Author Signature

12/14/2023
Date